Photodiagnosis and Photodynamic Therapy 25 (2019) 177–192

Contents lists available at ScienceDirect

Photodiagnosis and Photodynamic Therapy

journal homepage: www.elsevier.com/locate/pdpdt

Review

Advances in the application of upconversion nanoparticles for detecting and treating cancers

Kunmeng Li[b,1], Enlv Hong[b,1], Bing Wang[c,1], Zhiyu Wang[b,1], Liwen Zhang[b], Ruixia Hu[b], Baiqi Wang[a,b,d,*]

[a] The Key Laboratory of Modern Toxicology of Ministry of Education, Nanjing Medical University, Nanjing, 211166, Jiangsu, China
[b] Department of Occupational and Environmental Health, School of Public Health, Tianjin Medical University, Tianjin, 300070, China
[c] Department of Ophthalmology, Fujian Medical University Union Hospital, Fuzhou, 350001, Fujian, China
[d] The Key Laboratory of Environment, Nutrion and Public Health of Tianjin, Tianjin Medical University, Tianjin, 300070, China

ARTICLE INFO

Keywords:
Upconversion nanoparticles
Cancer detection
Cancer therapy

ABSTRACT

The detection and treatment of cancer cells at an early stage are crucial for prolonging the survival time and improving the quality of life of patients. Upconversion nanoparticles (UCNPs) have unique physical and chemical advantages and likely provide a platform for detecting and treating cancer cells at an early stage. In this paper, the principle of UCNPs as chemical sensors based on fluorescence resonance energy transfer (FRET) has been briefly introduced. Research progress in such chemical sensors for detecting and analyzing bioactive substances and heavy metal ions at the subcellular level has been summarized. The principle of UCNP-based nanoprobe-targeting of cancer cells has been described. The research progress in using nanocomposites for cancer cell detection, namely cancer cell targeted imaging and tissue staining, has been discussed. In the field of cancer treatment, the principles and research progress of UCNPs in photodynamic therapy and photothermal therapy of cancer cells are systematically discussed. Finally, the prospects for UCNPs and remaining challenges to UCNP application in the field of cancer diagnosis and treatment are briefly described. This review provides powerful theoretical guidance and useful practical information for the research and application of UCNPs in the field of cancer.

1. Introduction

Cancer forms malignant tumors that seriously threaten human life and health [1]. It is estimated that 1,735,350 new cases of cancer will be diagnosed in the United States in 2018, with an average of 4700 cases per day, leading to 609,640 deaths from cancer and 1700 deaths each day [2]. Currently, cancer patients are often in advanced stages when they are diagnosed. These patients have missed the best treatment stage because the cancer cells have already undergone large-scale metastases in the body. If cancer can be diagnosed and treated at an early stage, existing technical conditions can be used to effectively control the condition and greatly reduce mortality [3]. Therefore, in the field of life science, it is of great practical significance to achieve early diagnosis and therapy of cancer.

In recent years, nanotechnology has rapidly developed and shown enormous application potential in the biomedical field [4]. Nanotechnology has been explored to seek a breakthrough in the diagnosis and treatment of malignant tumors [5]. Among the numerous nanomaterials developed, rare-earth upconversion nanoparticles (UCNPs) have attracted widespread attention because of their unique advantages [6]. Upconversion luminescence (UCL) of rare-earth doping is an anti-Stokes process and generally refers to a process in which rare-earth ions

Abbreviations: AlPcS4, *tetra*-sulfonicphthalocyanine aluminum; AuNP, sgold nanoparticles; Au-UCNP, gold-UCNPs; CD, circulardichroism; Ce6, Chlorine6; CH, chitosan; csUCNP@C, NaLuF4:Yb,Er@NaLuF4@Carbon; A (conA), Concanavalin; CT, computedX-ray tomography; FA-Gd-Si-TiNPs, folic acid-targeted $NaGdF_4$:Yb/Tm@SiO_2@TiO_2 nanocomposites; FRET, Fluorescenceresonant energy transfer; IgG, immunoglobulinG; MFNPs, multifunctionalnanoparticles; miRNA, microRNA; MRI, magneticresonance imaging; NIR, near-infrared light; NPs, nanoparticles; NRD, Nilered derivative; PAA, polyacrylicacid; PDT, photodynamic therapy; PEI, polyethyleneimine; PET, positronemission tomography; PS, photosensitizers; PTT, photothermaltherapy; siRNA, smallinterfering RNA; SPECT, single-photon emission computed tomography; SPIONssuperparamagnetic, iron oxides; UCL, upconversionluminescence; UCNPs, upconversion nanoparticles; UV, ultraviolet; ZnPc, Zn (II)-phthalocyanine

* Corresponding author at: No. 22, Qixiangtai Rd., Heping District, Tianjin, 300070, China.
E-mail address: wbqpaper@126.com (B. Wang).
[1] These authors contributed equally to this work.

https://doi.org/10.1016/j.pdpdt.2018.12.007
Received 12 July 2018; Received in revised form 12 December 2018; Accepted 19 December 2018
Available online 21 December 2018
1572-1000/

successively absorb two or more long-wavelength photons and emit short-wavelength, high-energy photons. Stokes' process is the process by which high-energy photons excite low-energy photons [7]. However, it was later discovered that some materials can achieve the opposite of this law of luminescence effects, which was referred to as anti-Stokes luminescence, or UCL [8].

Upconversion nano-rare-earth luminescent material is a classic anti-Stokes luminescent material. Upconversion was first reported in the 1950s when researchers excited polycrystalline ZnS with 960-nm near-infrared light and observed green light emission. In 1962, similar phenomena were observed for selenide compounds. In 1966, when studying lanthanum tungstate glass, Auzel found that when Yb^{3+}, Ho^{3+}, Er^{3+}, and Tm^{3+} were incorporated into a host material, the visible light emission intensity increased by 2–3 orders of magnitude following excitation with infrared light [9]. This paper formally introduced the idea of UCL. The UCL mechanism mainly includes the four processes of excitation state absorption, energy transfer, direct two-photon absorption, and photon avalanche. Numerous reviews and studies have addressed the UCL mechanism [10–12].

UCNPs continuously absorb long-wavelength photons (such as near-infrared light) and then radiate short-wavelength photons via two-photon or multiphoton mechanisms [13,14]. Therefore, UCNPs have many advantages for application in biological systems compared to conventional organic fluorescent dyes. First, in human tissue, some enzymes and nucleic acids absorb ultraviolet light, resulting in tissue degeneration or damage. However, the excitation light of the UCNPs is typically in the near-infrared region, and UCNPs absorb near-infrared light. Therefore, using near-infrared light as an excitation light source not only prevents damage to normal tissues but also shows deep tissue-penetrating ability and can effectively avoid interference from the fluorescence of the living body itself. Second, UCNPs with a large Stokes shift, weak photobleaching, low toxicity, and good stability have high potential for applications as integrated probes for diagnosis and treatment. Finally, the emission spectrum of the UCNPs can achieve modulation from the ultraviolet region to the visible region and near-infrared region [15,16]. The unique properties of UCNPs facilitate their complexation with other nanomaterials, such as gold nanoparticles, carbon dots, fluorescent dyes, photosensitizers, graphene, and graphene oxide [17–19]. UCNPs absorb the emission from these nanomaterials via fluorescence resonance energy transfer (FRET) and thus can be used in related fields.

These advantages give UCNPs broad application potential in the field of biomedicine, particularly for the early diagnosis and treatment of cancer [20,21], as demonstrated in numerous studies. There are many reviews describing the systematic synthesis, characterization, and application of UCNPs [22–24]. However, there are relatively few systematic reviews of UCNPs in the field of cancer, preventing their application by researchers in the field of nano-oncology [25–27]. Therefore, we systematically classified and described recent studies of UCNPs in the field of cancer diagnosis and treatment. We first introduce the principle of FRET based on UCNPs and summarize the application of UCNPs for analyzing biologically active substances and heavy metal ions at the subcellular level. Next, we describe the use of UCNPs for cell detection, focusing on targeting cancer cell imaging, multimodal imaging of cancer cells, and UCNPs for *in vivo* and *in vitro* photodynamic therapy (PDT) and photothermal therapy (PTT) of cancer cells. Finally, problems of and challenges related to using UCNPs for cancer detection and treatment are described. This article provides powerful theoretical guidance for researchers in the field of nano-oncology.

2. Biological detection

In recent years, chemical biosensors based on the principle of FRET have been widely used in biomedical and other fields [28,29]. FRET is a mechanism in which energy transfer occurs between two light-sensitive molecules (chromophores). A donor chromophore, initially in its electronic excited state, may transfer energy to an acceptor chromophore through nonradiative dipole–dipole coupling. FRET efficiency can be measured to determine whether two fluorophores are within a certain distance of each other. These measurements are used in studies in the fields of biology, chemistry, and nano-oncology.

FRET is an important method for adjusting the UCL emission spectra of multicolor imaging [30]. By coupling UCNPs with metal nanoparticles (such as Au nanoparticles) or organic fluorophores, FRET can be achieved. Using UCNPs as donors and fluorophores or Au nanoparticles as receptors, researchers can design chemical sensors with high sensitivity for detecting biological molecules [31]. In 2005, Li et al. first conducted FRET based on UCNPs for biological detection [32].

Since then, an increasing number of studies of various biosensor-related studies based on the FRET principle has been conducted. Zijlmans and collaborators first conjugated UCNPs with NeutrAvidin. The conjugate was successfully used to detect prostate-specific antigen in tissue sections and the CD4 membrane antigen on human lymphocytes [33]. In a FRET system, when absorption of the energy acceptor is close to the emission of the phosphor and donor and the acceptor are close enough, emission from the energy donor (UCNPs) will be quenched by the energy acceptor. According to this theory, Wang and coworkers fabricated a FRET system that combined $Na(Y_{1.5}Na_{0.5})F_6:Yb^{3+},Er^{3+}$ UCNPs and gold nanoparticles. The FRET system sensitively detected trace amounts of avidin [32]. Mao et al. used $NaYF_4$:Yb, Er UCNPs (30–70 nm in diameter) and gold nanoparticles (Au NPs, 18–33 nm in diameter) to develop a sandwich-type FRET system for detecting goat antihuman immunoglobulin G (IgG). The fluorescence change in the FRET system was linearly correlated with the concentration of goat antihuman IgG in the range of 3–67 $\mu g \cdot mL^{-1}$. The detection limit of the system was low, reaching 0.88 $\mu g \cdot mL^{-1}$. This study demonstrated that the fabricated FRET system was applicable for detecting trace proteins (Fig. 1) [34]. Liu and his team constructed a novel sensor based on FRET from PAA-functionalized $NaYF_4$:Yb,Er UCNPs (particle size of approximately 50 nm) to graphene oxide (GO). The fabricated FRET system sensitively detected glucose in serum samples without background interference (Fig. 2) [35].

Based on the principle of FRET, a sensor built on the UCNP surface modified with the proper molecules for detection in the biological and chemical field and showed good application prospects. Duan and his team synthesized facial layer-by-layer engineered UCNPs for near-infrared (NIR)-initiated tracking and the delivery of small interfering RNA (siRNA) to ovarian cancer cells showing multidrug resistance (MDR).

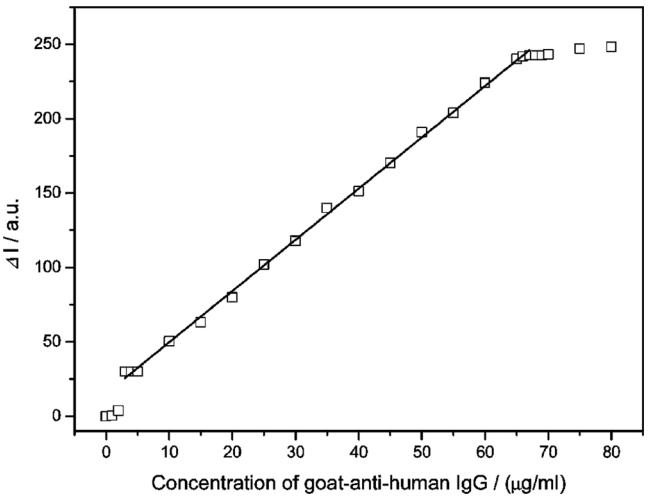

Fig. 1. Linear relationship between the quenching of UC fluorescent intensity (ΔI) at 542 nm and concentration of goat antihuman IgG. (Reprinted with permission from ref. [34]. Copyright 2009 American Chemical Society).

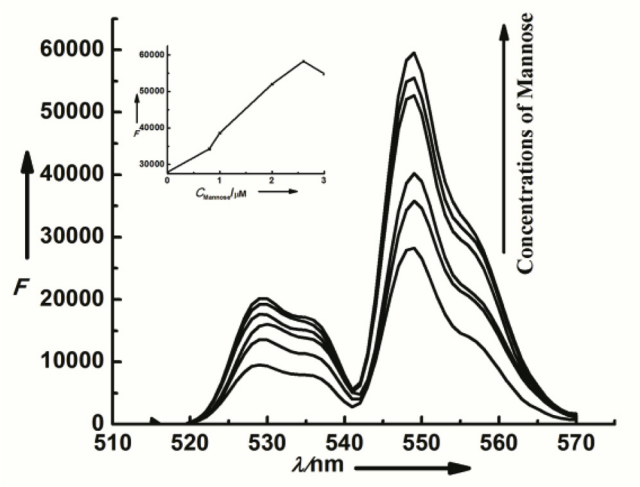

Fig. 2. Fluorescence emission spectra of the GO-CS-ConA-UCP complex in the presence of different concentrations of mannose (0.8–3.0 μM) in Tris-HCl (0.01 M, pH 7.4) buffer. Inset: mannose concentration dependence of UCP fluorescence. (Reprinted with permission from ref. [35]).

The delivery vehicle enhanced the cellular uptake of MDR1-siRNA, protected MDR-siRNA from nuclease degradation, and promoted endosomal escape to silence the MDR gene. The UCNPs were used to monitor the MRD1-siRNA biological process by NIR- initiated FRET between the donor UCNPs and acceptor fluorescence dye-labeled MDR1-siRNA [36]. Kuang et al. fabricated DNA-driven gold nanoparticles (Au NPs, 20 ± 3 nm, aspect ratio 1:1.2) and $NaGdF_4$:Yb^{3+},Er^{3+} UCNPs

(UCNP, 19 ± 3 nm) pyramids to detect microRNA (miRNA) in real-time. The Au-UCNP pyramids displayed strong plasmonic circular dichroism (CD) at 521 nm and significant luminescence at 500–600 nm. They demonstrated that the CD intensity had an outstanding linear range from 0.073 to 43.65 fmol/10 μg_{RNA} and limit of detection of 0.03 fmol/10 μg_{RNA}, whereas the luminescence intensity ranged from 0.16 to 43.65 fmol/10 μg_{RNA} with a limit of detection of 0.12 fmol/10 μg_{RNA}. This method provided a new approach for ultrasensitive detection and quantification of miRNA in living cells (Fig. 3) [37].

Based on a similar principle, UCNPs showed very good potential for chemical detection. Zhang and his collaborators synthesized thiazole-derivative- functionalized $NaYF_4$:20%Yb,1.8%Er,0.5%Tm UCNPs (average diameter of approximately 25 nm). They used the upconversion emission intensity ratio as a ratiometric signal to analyze Hg^{2+} in living cells. The results demonstrated that the prepared nanosystem could be used to monitor changes in Hg^{2+} in living cells with low cytotoxicity (Fig. 4) [38]. Sun and co-workers prepared a fluorescent probe by conjugating Nile red derivative (NRD) with polymer-modified $NaGdF_4$-coated $NaYF_4$:Yb,Er,Tm UCNPs (approximately 41 in diameter). In this nanostructure, the UCNPs served as the energy donor while NRD was the energy acceptor, leading to efficient FRET. These FRET nanoprobes exhibited high selectivity and sensitivity for detecting Fe^{3+} in water and living cells (Fig. 5) [39]. Liu and his team constructed a new UCNP probe through

< InlineShape1 > heavy metal ion-induced quenching. Their results showed that heavy metal ions could quench the UCL by > 95% without spectral overlap. This nanoprobe was able to sensitively detect biothiols in living cells and tissues and was a powerful tool for studying biological events associated with changes in biothiol contents [40].

Other groups carried out detection of nucleic acid, DNA, glucose, and human chorionic gonadotropin using UCNPs and obtained promising results [41–44]. Liu and co-workers constructed a new type of pH sensor using UCNPs as the core and silica as the shell to graft bovine serum albumin as another shell (UCNPs@SiO_2@BSA). This core-shell-shell structure provides a large surface for loading various pH-sensitive dyes, such as bromothymol blue and rhodamine B. The sensitivity of a sensor with this structure is several tens of fold greater than the sensitivity of the ratio fluorescence method while retaining good stability in a high-ionconcentration environment. Because the use of near-infrared excitation light at 980 nm can effectively avoid the background fluorescence interference of biological samples, the prepared sensor can be widely applied for pH detection in various biological samples [45]. Other research groups carried out similar studies and achieved satisfactory results [46–49].

3. Detection of cells

Upconversion luminescent nanomaterials have a high signal-to-noise ratio and sensitivity in biology and tumor cell imaging because of the lack of background fluorescence interference. Studies of UCNPs for staining imaging at the cellular level first began in 1999. Zijlmans et al. used the (Y.Yb.Tm)O_2S and (Y.Yb.Er)O_2S (with a size distribution of 200–400 nm) with different luminescent colors to convert phosphorescent nanoparticles for imaging of cells and to stain tissue sections [33]. They compared the results of UCNPs with those obtained using the conventional dye molecule fluorescein isothiocyanate. The results showed that fluorescein isothiocyanate imaging exhibited strong background fluorescence even in the absence of cells, which was not observed for UCNPs. Additionally, they studied the fluorescence stability of UCNPs and observed no photobleaching phenomenon in the nanoparticles, indicating that UCNPs are particularly suitable for long-term tracking applications of cancer cells. Zhang and collaborators synthesized silicon-encapsulated UCNPs for use as cell-tracking imaging reagents. After injecting the UCNPs into mice through the tail vein, a signal was observed from the UCNPs in the ear vessels of the mice

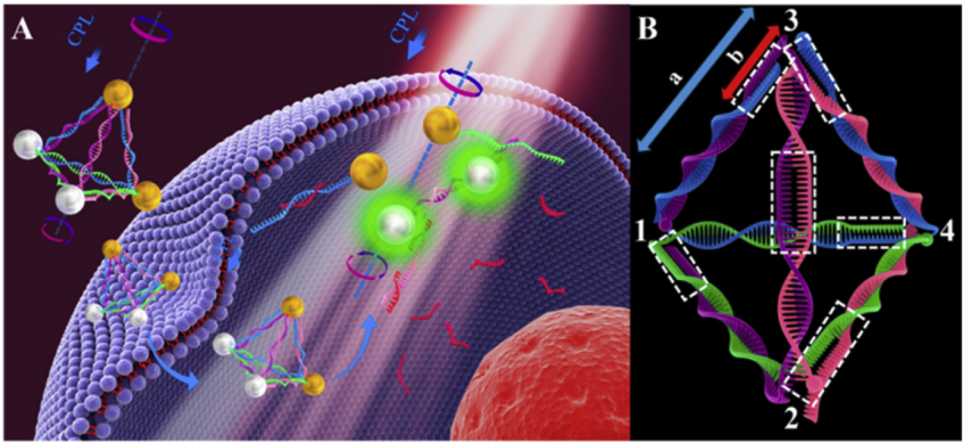

Fig. 3. (A) Working principle of Au-UCNP pyramids for miRNA detection and (B) nucleic acid skeleton of pyramid used for miRNA detection[a] a3, 4 are linked with Au NPs; 1, 2 are linked with UCNPs. Part a: Recognition sequence of miRNA; part b: non-complemented part (enclosed by white dashed line). (Reprinted with permission from ref. [37]. Copyright 2016 American Chemical Society).

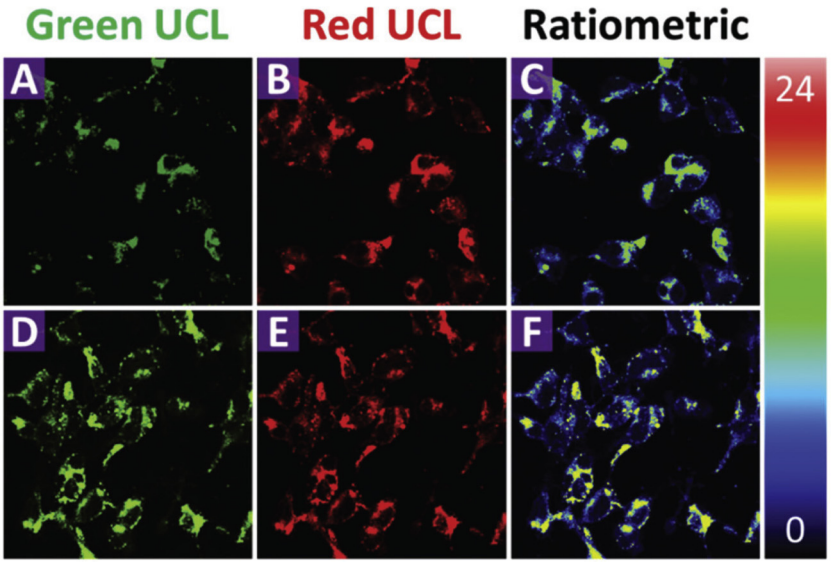

Fig. 4. Ratiometric UCL images in HeLa cells (top, A–C) and 200 μM Hg^{2+}-treated HeLa cells (bottom, D–F) incubated with 0.5 mg mL^{-1} of 2-UCNPs for 180 min. Emission was collected by both the green channel at 500–560 nm (A and D) and red channel at 600–700 nm (B and E). (C and F) Ratiometric UCL images with the ratio of green to red channels. (Reprinted with permission from ref. [38]).

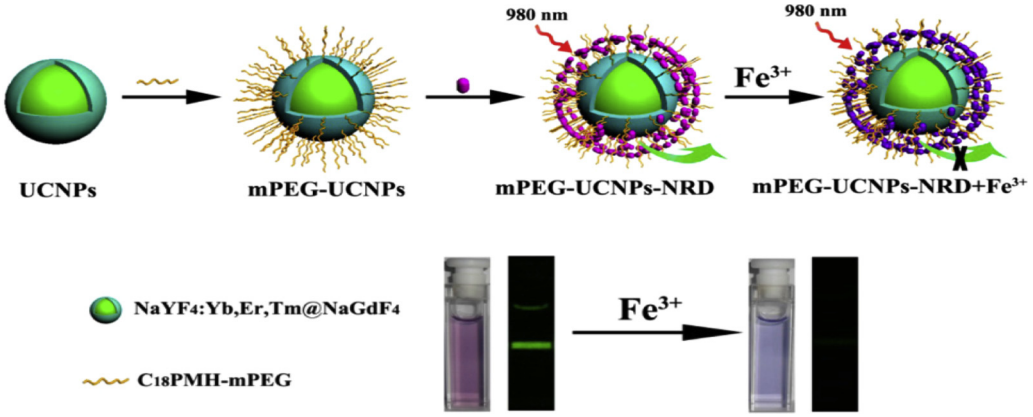

Fig. 5. mPEG-UCNPs-NRD and their application in detecting Fe^{3+} based on changes in UCL emission (Reprinted with permission from ref. [39]. Copyright 2016 American Chemical Society).

[50,51]. Since then, UCNP imaging has attracted wide attention, and related research reports have increased rapidly [52,53].

At the imaging level of living tissue, Lim et al. first imaged the digestive system of the nematode worm *Caenorhabditis elegans* using UCNPs [54]. In 2007, Zhang and his group first demonstrated the application of UCNP-based PDT in MCF-7/AZ breast cancer cells [55]. In 2008, Zhang and co-workers subcutaneously injected PEI-coated $NaYF_4$:Yb,Er and PEI-modified $NaYF_4$:Yb,Tm UCNPs with a particle size of approximately 50 nm into mice. Fluorescence imaging was conducted to observe the distribution of UCNPs in mice under NIR excitation at 980 nm [56]. In the same year, the Nyk team first conducted UCL imaging in BALB/c mice by observing the distribution of UCNPs following intravenous injection into mice. The results showed that UCNPs were mainly distributed in the liver and spleen of the mice. Their experiments also demonstrated that UCL imaging does not exhibit tissue autofluorescence compared to conventional down-converted luminescent materials, such as quantum dots and organic dyes [57].

Additionally, UCNPs show minimal autofluorescence from biological tissues, enabling improved imaging sensitivity in biological systems. Therefore, UCNPs have attracted great attention as nanoprobes for tracking stem cells. Ma and co-workers synthesized and used $NaYF_4$:Yb^{3+},Er^{3+} UCNPs to label and tract rabbit bone marrow mesenchymal stem cells (rBMSCs). The prepared UCNPs nanoprobes effectively tracked rBMSCs during the osteogenesis process [58]. Zhao et al. prepared polythylenimine (PEI) covalently conjugated (α-$NaYbF_4$:Tm^{3+})/CaF_2 UCNPs (PEI-UCNP) and used the fabricated PEI-UCNP to label rat mesenchymal stem cells (rMSCs). Their study demonstrated that PEI-UCNP does not influence the normal early proliferation of rMSCs or leak from the cells. Moreover, PEI-labeled rMSCs cells underwent osteogenic and adipogenic differentiation upon *in vitro* induction [59]. Li and co-workers developed a multifunctional nanocarrier based on UCNPs, which was conjugated to the peptide (Cys-Arg-Gly-Asp, CRGD) and the differentiation- inducing kartogenin (KGN) via a photocaged linker. The luminescent UCNP nanoparticle carrier was used for long-term tracking of labeled hMSCs *in vivo*. Under NIR irradiation, chondrogenic differentiation of the subcutaneously implanted hMSCs treated with the built nanocarrier was induced. Their results demonstrated that UCNP nanocarriers are promising and powerful tools for studying the mechanism of stem cells *in vivo* [60]. Similarly, Liu et al. synthesized UCNPs as an exogenous contrast agent to track mouse MSCs *in vivo*. They found that as few as 10 cells labeled with UCNPs could be accurately detected *in vivo*. Thus, UCNPs are a new type of ultra-sensitive probe useful for labeling and tracking stem cells at nearly the single-cell level [61].

4. Tumor-targeted molecular imaging

Tumor-targeted molecular imaging plays a very important role in the diagnosis and treatment of cancers. Because of their unique optical properties, UCNPs are widely used for active targeted imaging of

tumors. In 2009, Li and co-workers were the first group to achieve UCNP-based tumor-targeted imaging [62]. In two different studies, they coupled UCNP with folic acid and RGD sequences [62,63]. After 1 day of intravenous injection of FA-UCNP into nude mice carrying HeLa cell tumors, significant UCL signals were observed at the tumor site, whereas no signal was observed in the control group. In a subsequent study, the research group connected a neurotoxin to the UCNP surface. Because neurotoxins have a high affinity for tumor cells, the nanoprobe achieved targeted UCL imaging of the tumor cells [64]. These studies confirmed that UCNP can be used as a molecular probe for targeting tumor diagnosis.

Based on antigen-antibody and ligand-receptor interactions, UCNPs can specifically label cells, thus enabling active targeting imaging. Zhang et al. used UCNPs to label cancer cells in 2008. They prepared PEI-coated $NaYF_4$:Yb,Er NPs, which are well-dispersed spherical NPs with a mean diameter of approximately 50 nm and can emit strong upconversion fluorescence under excitation with 980 nm photons. The PEI-coated UCNPs were further conjugated to folic acid to fabricate UCNP nanoprobes. The constructed UCNP nanoprobes accurately targeted human HT29 adenocarcinoma cells and human OVCAR3 ovarian carcinoma cells overexpressing folate receptors on the cell surface (Fig. 6) [56]. Mao and co-workers prepared amino-modified $NaYF_4$:Yb,Er UCNPs coated with silica. The prepared UCNPs were further combined with a rabbit anti-CEA8 antibody to form antibody-UCNP conjugates. Antibody-UCNP conjugates were used to effectively immunolabel and image HeLa cells and were examined in both *in vitro* and *in vivo* nanomedicine studies [65]. Shi and co-workers successfully developed stable upconversion immune- nanohybrids based on $NaYF_4$:20%Yb^{3+}/2%Er^{3+} UCNPs (27 ± 8.2 nm in diameter). The UCNP nanoprobes specifically detected prostate cancer cells with stable and background-free luminescent signals. This work provided a versatile strategy for developing a UCNP platform for sensitively detecting diseased cells (Fig. 7) [66].

Wang and Xu et al. prepared $NaYF_4$:Yb,Er UCNPs via a microwave-assisted solvothermal approach. The UCNPs were coupled with a CEA-8 antibody to form an immunobioprobe, which was successfully applied for specific fluorescent immunolabeling and imaging of HeLa cells [67]. Veggel and his collaborators synthesized PEG-coated core/shell $NaYF_4$ NPs through a chemical route. The NPs probes were used to image a line of ovarian cancer cells (CaOV3) [68]. Other groups also studied the use of UCNPs for labeling cancer cells and obtained promising results [69,70]

5. Multimodal imaging

With the development of medical imaging technology and improvement in clinical practical needs, single-modal imaging has become increasingly unable to meet the clinical needs. Therefore, multimodal imaging technologies are urgently needed. The imaging of traditional down-converting fluorescent material exhibits a serious photobleaching phenomenon and poor tissue penetration ability because it requires excitation with high-energy ultraviolet light. Additionally, down-converted nanomaterials are also susceptible to tissue autofluorescence interference and have low imaging sensitivity. UCL imaging shows no background fluorescence interference and has high imaging sensitivity, but its spatial resolution is low. Another important imaging technology, magnetic resonance imaging (MRI), is mainly tomography with strong tissue penetration, but the imaging sensitivity is low. Recently, new imaging technologies such as computed X-ray tomography (CT) imaging and positron emission spectroscopy (PET)-single-photon emission CT (SPECT) imaging have been developed very rapidly. Next, based on the conversion fluorescence imaging described above, combined with other imaging methods, we briefly summarize the progress of multimodal imaging based on UCNPs.

Multimodal imaging combines several different imaging modes to overcome the limitations of each single imaging method. Multimodal imaging technology has received much attention in the field of biomedical imaging. Gd^{3+} compounds are a very effective class of magnetic resonance contrast agents. By doping with the element Gd, many upconversion materials are endowed with both UCL imaging and MRI capabilities. Hyeon's group achieved dual-modal imaging of breast cancer cells (SK-BR-3) using $NaGdF_4$:Yb/Er upconverting UCNPs (Fig. 8) [71].

Li's research group prepared a water-soluble $NaGdF_4$ upconversion luminescent nanomaterial by oxidizing the surface of oleic acid. The UCNPs were used for MRI/UCL dual-modal imaging at the living body level, exhibiting high imaging sensitivity without significant biological toxicity [72]. Subsequently, the research team used radioactive ^{18}F to replace some of the F ions in $NaGdF_4$ to prepare a multifunctional upconversion luminescent nanomaterial. The UCNPs successfully

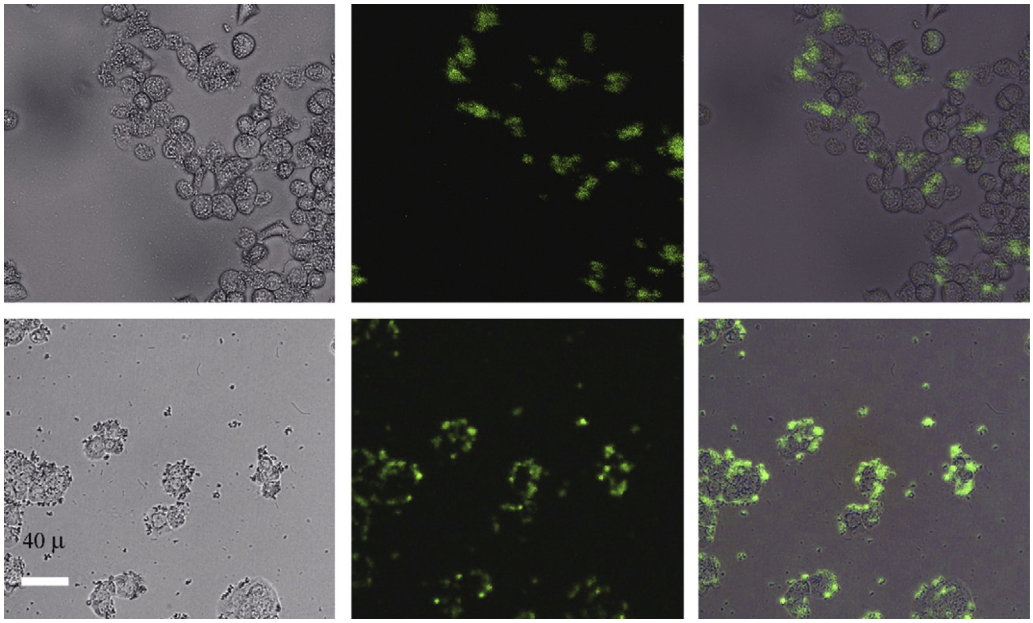

Fig. 6. Bright field, confocal, and superimposed images of live human ovarian carcinoma cells (OVCAR3, top row) and human colonic adenocarcinoma cells (HT29, bottom row), with PEI/$NaYF_4$ nanoparticles attached. The nanoparticles were surface-modified with folic acid. (Reprinted with permission from ref. [56]).

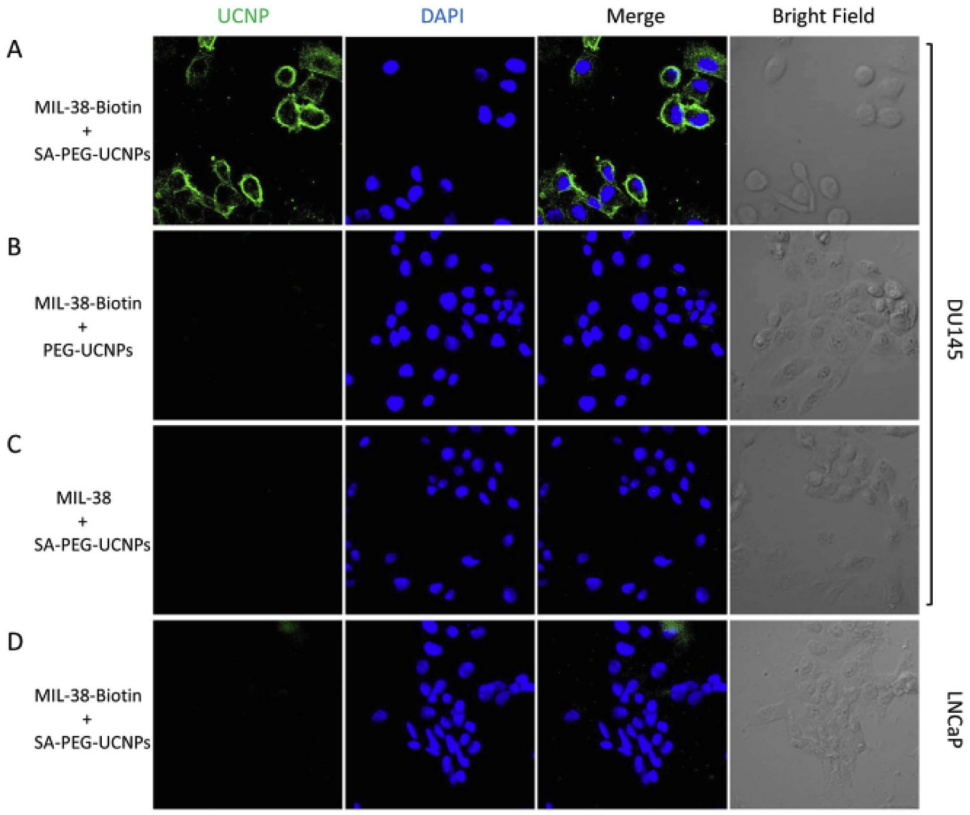

Fig. 7. Confocal upconversion fluorescence imaging of (A) SA-PEG-UCNPs + biotinylated MIL-38 (MIL-38-Biotin)-labeled DU145 prostate cancer cells; (B) PEG-UCNPs + MIL-38-Biotin-labeled DU145 prostate cancer cells; (C) SA-PEG-UCNPs + MIL-38-labeled DU145 prostate cancer cells; (D) SA-PEG-UCNPs + MIL-38-Biotin-labeled LNCaP prostate cancer cells. Green and blue colors represent upconversion fluorescence signals and blue fluorescence from UCNPs and DAPI, respectively. (Reprinted with permission from ref. [66]).

achieved trimodal imaging via UCL/MRI/radioactive labeling for the first time at the living body level [73].

Prasad and co-workers synthesized $NaYF_4$ nanoparticles co-doped with various rare-earth ions (Eu^{3+}, Er^{3+}, Yb^{3+}, Gd^{3+}). The prepared UCNPs (size distribution in the range of 25–30 nm) were colloidally stable and easily detectable by both MR and optical imaging. These UCNPs were further functionalized by anti-claudin 4. The fabricated UCNPs exhibited excellent targeted imaging of living cancer cells under MR and optical modes (Fig. 9) [74]. They next fabricated an $NaGdF_4$ shell on the surface of $NaYbF_4$:Tm^{3+} nanocrystals, which resulted in an

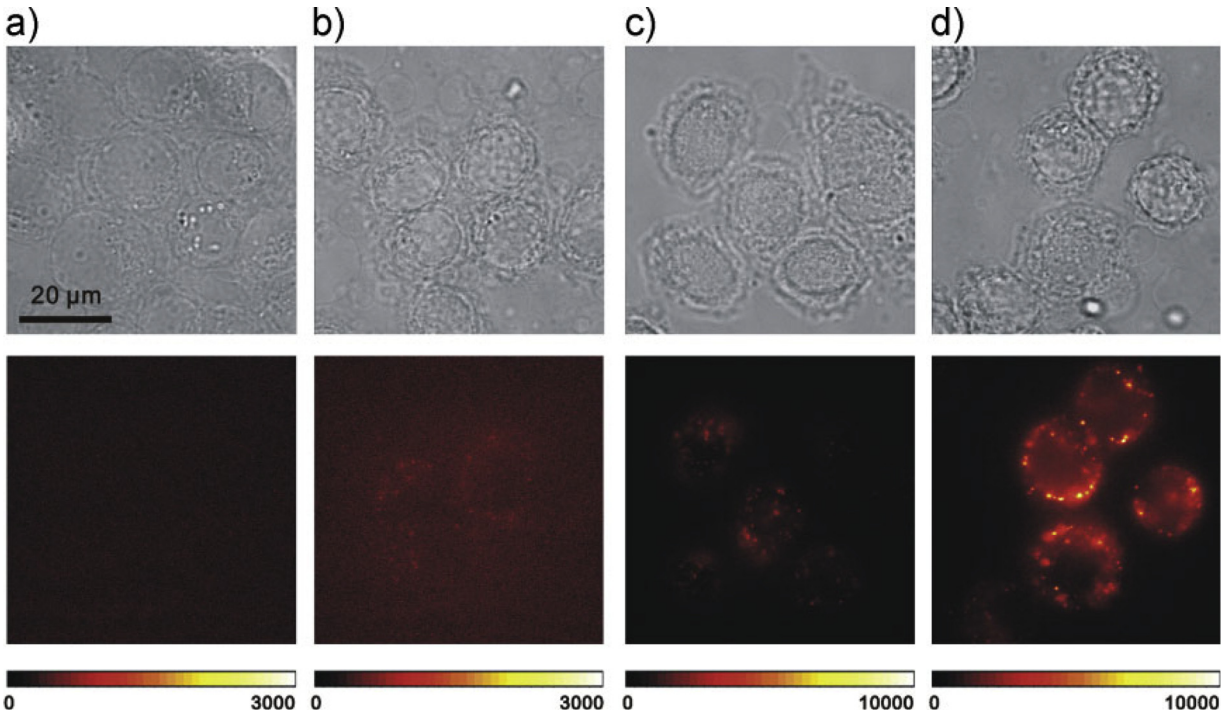

Fig. 8. Cellular uptake of 20-nm UCNPs in SK-BR-3 cells. (Top row) Bright field images. (Bottom row) Luminescence images with the excitation at 980 nm and the detection at 400–700 nm. Cells were incubated with the UCNPs with 100 mg μL^{-1} of Gd^{3+} concentration at 37°C. a) Cells incubated without UCNPs, showing no autofluorescence. Incubation time was b) 30 min, c) 2 h, d) 4 h. (Reprinted with permission from ref. [71]).

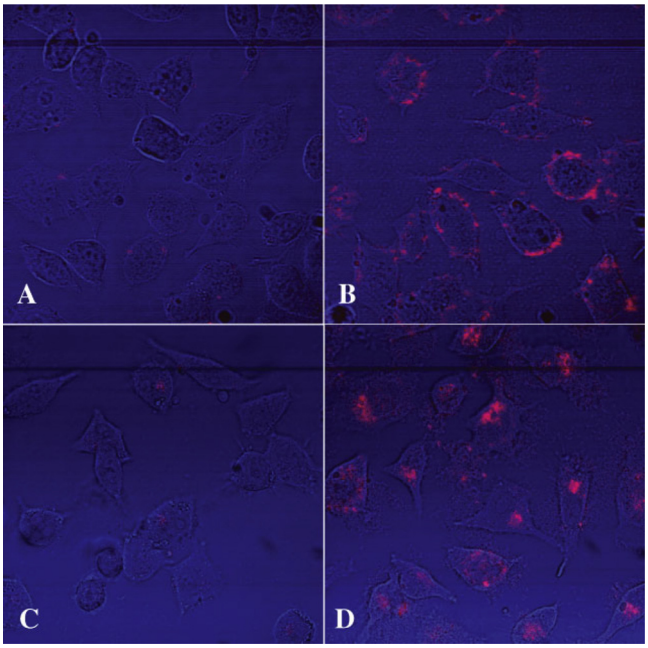

Fig. 9. Confocal images of Panc 1 cells treated with UCNPs ($NaYF_4$: 2% Er^{3+}, 10% Yb^{3+}, 10% Gd^{3+}; A, B) and DCNPs ($NaYF_4$: 10% Eu^{3+}, 10% Gd^{3+}; C, D). (A) and (C) show non-bioconjugated nanophosphors, (B) and (D) show cells targeted with nanophosphors conjugated with anti-claudin 4 and anti-mesothelin, respectively. (Reprinted with permission from ref. [74]).

approximately three-fold increase in the fluorescence intensity of the UCNPs. The UCNPs probes are an efficient contrast agent because of the combined presence of optical and MR imaging capabilities [75]. Li and collaborators prepared core-shell structured $NaYF_4$:Yb^{3+},Tm^{3+}@Fe_xO_y nanocrystals, which integrated UCL and magnetic function in a nanoparticle. The prepared nanoparticles were used to accurately label KB cells by MR and UCL dual-modal imaging [76].

Compared to the limitation of low sensitivity and relatively low penetration in tissue of luminescence, PET shows the highest sensitivity and tissue penetration and is widely used for bioimaging *in vivo* in living subjects. Therefore, Zeng and co-workers prepared sub-10-nm $BaLaF_5$:Mn/Yb/Er UCNPs for dual-modal X-ray and UC imaging using a solvothermal method. The UCNPs were used to label HeLa cells. In *in vivo* experiments, simultaneous X-ray and UC imaging of a nude mouse illustrated that the UCNPs nanoprobes were effective dual-modal bioprobes [77]. Shi and co-workers fabricated silica-shielded, magnetic upconversion, fluorescent oligomers with controlled particle size and size distribution. They subcutaneously injected the silica-shielded, magnetic upconversion, fluorescent oligomer probes into the tumor site and obtained satisfactory dual-modal MRI and upconversion imaging results [78]. Li and his collaborators prepared ^{18}F-labeled rare-earth nanoparticles ($NaYF_4$:Yb^{3+},Tm^{3+}, approximately 20 nm in diameter) through a facile inorganic reaction between rare-earth cations and fluoride ions. The UCNPs exhibited good imaging capability for mice using the UCL/PET modality (Fig. 10) [79]. Yang et al. used a similar technique to synthesize $NaLuF_4$:^{153}Sm,Yb,Tm nanoparticles. These UCNPs exhibited very low cytotoxicity and excellent *in vitro* and *in vivo* performance in UCL/SPECT dual-modal imaging. The dual-functional UCNPs provided a facile platform for ultra-sensitive molecular imaging on the cellular scale to the whole-body level [80].

Shao and co-workers developed a Fe_3O_4@$NaLuF_4$:Yb,Er/Tm nanophosphor (MUCNP), which integrated upconversion luminescence, magnetic, and X-ray attenuation properties. The MUCNP displayed good performance in MR, CT, and UCL *in vivo* to obtain images of human cervical carcinoma (HeLa cell)-bearing mice [81]. Liu and co-workers used a similar approach to prepare oleic acid, aminocaproic acid, and folic acid functionalized UCNPs. Before these ligands were coated onto the surface of UCNPs, Gd^{3+} was doped on the UCNPs through cation exchange. Moreover, radioactive $^{18}F^-$ for PET imaging was integrated on the UCNPs via interactions with rare-earth ions. The constructed UCNPs showed excellent upconversion luminescence properties, MR, radioactivity, targeted function, and biocompatibility. The multifunctional UCNPs were used to label breast cancer cells for cellular targeted imaging, MRI, *in vivo* upconversion luminescence, and PET imaging [82].

The combination of nanotechnology with optical, CT and MRI technology can overcome the limitations of single imaging technology and combine the advantages of several imaging technologies, and has great application potential in the field of tumor diagnosis and treatment. Therefore, Deng and co-workers constructed a multimodal PEGlated Mn^{2+}-doped $NaLuF_4$:Yb/Er nanocontrast agent with deep tissue imaging as well as excellent UCL, CT, and MRI imaging capabilities. Additionally, surface modification with PEG gives this nanoprobe excellent biocompatibility for applications in clinical practice [83]. Therefore, the dual-modal and multimodal UCNP probes show great potential for use in early cancer diagnosis [84–87].

6. PDT based on UCNPs

The UCNPs can convert two or more low-energy NIR photons into a higher-energy photon through a non-linear anti-stokes process [88,89]. The combination of UCNPs with other functional moieties can endow them with highly enriched functionalities for imaging-guided cancer treatment [90–92]. The UCNPs may also be combined with anti-cancer drugs, photosensitizers (PS), or gold nanostructures for potential therapeutic application, including chemotherapy, PDT, and PTT [93]. Integrated UCNPs, which have emerged as a new class of theranostic agents in biomedicine, have attracted wide attention. They provide a completely new platform for the detection and treatment of cancer cells.

PDT has been successfully used for treating cancers [94,95]. Three major components are involved in PDT: light, photosensitizer, and oxygen. Upon excitation by a designed wavelength of light, photosensitizers can be selectively activated to generate cytotoxic ROS to induce cancer cell death [96,97]. Traditional photosensitizer molecules are often excited by visible or ultraviolet light, which is in the region of strong optical absorption and scattering in biological tissue. In contrast, the excitation light of UCNPs is in the near-infrared waveband and has deeper penetration depth in the tissue. Additionally, nanomaterials can carry photosensitizers or other drugs due to their unique physical and chemical properties, thus improving the efficiency of targeted delivery of the photosensitizer and PDT.

To date, numerous studies of PDT based on UCNPs have been reported. Zhang et al. prepared $NaYF_4$:25%Yb^{3+}, 0.2%Er^{3+} oleic acid coated UCNPs (average diameter of approximately 30 nm) combined with Zn(II)-phthalocyanine (ZnPc) PS, which exhibited highly efficient singlet oxygen generation. The high $^1O_2$ production led to efficient PDT treatment of liver tumors in mice. Moreover, the short irradiation duration was effective for image-guided PDT and inhibited liver tumor formation (Fig. 11) [98]. Wang and co-workers loaded Chlorin e6 (Ce6) onto polymer-coated UCNPs to form a UCNP-Ce6 supermolecule complex. Excellent PDT efficacy was achieved in 4T1 murine breast cancer upon intratumoral injection of UCNP-Ce6 under NIR excitation [99]. Zeng and co-workers synthesized tetra-sulfonic phthalocyanine aluminum ($AlPcS_4$) photosensitizer-conjugated Fe_3O_4@NaY_4:Yb:/Er (NPs-$AlPcS_4$) nanocomplexes. Under excitation irradiation at 980 nm, up to 70% of the MCF-7 cells incubated with NPs-$AlPcS_4$ were killed [100]. Later, the same group further constructed FA-targeted $NaGdF_4$:Yb/Tm@SiO_2@ TiO_2 nanocomposites (FA-Gd-Si-Ti NPs) for *in vivo* MRI and PDT. The obtained nanocomposites not only exhibited T-weighted MRI performance but also showed a clear signal in MCF-7 tumors. Under irradiation with a 980-nm laser, the viability of HeLa and MCF-7 cells

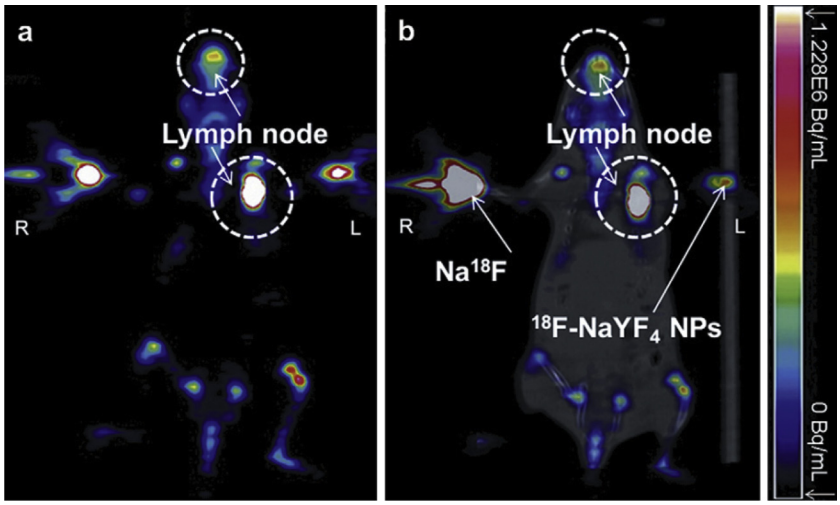

Fig. 10. PET imaging (a) and PET/CT imaging (b) of lymph node 30 min after subcutaneous injection of ^{18}F-UCNPs. Thirty minutes after subcutaneous injection of 740 kBq/0.05 mL ^{18}F-UCNPs into the left paw footpad, the signal in the lymph node reached its peak intensity, which was maintained for 60 min post-injection. In contrast, as a control free ^{18}F ions injected into the right paw showed no lymphatic imaging ability. (Reprinted with permission from ref. [79]).

dramatically decreased. Moreover, for *in vivo* PDT of MCF-7 tumor-bearing nude mice, the inhibition ratio of mice injected with FA-Gd-Si-Ti NPs reached 88.6% after 2 weeks of treatment [101]. To avoid the overheating effects of UCNPs, they further constructed an 808-nm-excited upconversion nanocomposite (T-UCNPs@Ce6@mSiO_2). The nanoprobes greatly improved the uptake by HER2-positive cells and tumors and showed excellent MRI and PDT efficacy in MDA-MB-435 tumor-bearing nude mice [102].

Li and co-workers built a core/shell structure of Yb/Tm/GZO@SiO_2 UCNPs, which can produce a multistep cascade energy transfer from the silica shell to Ga-doped Yb/Tm/ZnO. Compared to the UCL of Yb/Tm/ZnO UCNPs, the UCL intensity of Yb/Tm/GZO@SiO_2 was enhanced by approximately seven-fold. Under excitation with a 980-nm laser, the upconversion energy transfer efficiency of the UCL-optimized core/shell UCNPs was as high as 81%, and showed excellent PDT effects on HeLa cells [103].

Han and co-workers developed highly Yb-doped UCNPs with a biocompatible CaF_2 shell. 5-Aminolevulinic acid and protoporphyrin IX were further conjugated with UCNPs. The nanocomposites exhibited strong singlet oxygen generation and up to 70% cell death after 20 min of NIR irradiation. Additionally, the nanocomposites significantly reduced the tumor size even at below 12 mm in pork tissue in *in vivo* experiments using mice models [104]. Liu et al. prepared magnetic and fluorescent UCNPs for simultaneous MRI/UCL dual-imaging and PDT. The prepared UCNPs were not only useful for imaging of nasopharyngeal carcinoma CNE-2 cells but also achieved excellent PDT effects [105]. Scientists have shown that the spectral mismatch between the upconverted emission maximum of UCNPs and absorption maximum of most available photosensitizers greatly limits the therapeutic efficacy of UCNP-PDT platforms. Sha and co-workers fabricated a UCNP-PDT platform excited with biobenign 808-nm NIR which showed strong spectral overlap between the UCNP emission and absorption of zinc phthalocyanine photosensitizers. The prepared UCNP-PDT platform rapidly generated cytotoxicity under NIR excitation at an extremely low laser power density of only 0.6 W/cm^2. HeLa cancer cell spheroids 3 mm in diameter were effectively suppressed with a 65% decrease in cell viability following treatment with a UCNP-PDT platform. The spectrally matched UCNP-PDT platforms exhibited high suitability and effectiveness for cancer therapeutics [106].

Additionally, Liu and co-workers rationally designed a type of multi-tasking nanoparticle based on UCNPs. They simultaneously loaded Ce6, a photosensitizer, and imiquimod (R837), a Toll-like receptor 7 agonist, onto UCNPs. The UCNP-Cd6-R837 nanoparticles not only were useful for NIR-induced PDT to directly destroy mouse colon adenocarcinoma cell line (CT26) cells, but also stimulated immune responses by triggering dendritic cell maturation and cytokine secretion. Combined with this with CTLA4 checkpoint blockage therapy, the fabricated UCNPs efficiently eliminated tumor cells directly exposed to PDT and inhibited distant tumors left behind after PDT by exerting strong anti-tumor immune responses [107]. Similar studies also demonstrated that UCNPs are an excellent facile PDT platform for treating cancer cells [108–110].

7. PTT based on UCNPs

PTT is another effective approach for cancer treatment. During this process, UCNPs absorb photon energy and dissipate the absorbed energy into the surrounding solution via intrinsic-to-external phonon-phonon coupling, with subsequent local overheating, which can induce protein denaturation and further kill tumor cells. Under dark conditions, non-toxic PTT reagents can be used for tumor targeting through careful design. Local irradiation by light at the tumor site can achieve the dual point of selective treatment. Therefore, compared with chemotherapy, PTT has good selectivity and specificity and a low incidence of side effects.

Among the various nanomaterials, superparamagnetic iron oxides (SPIONs) are another class of widely studied nanomaterials in MRI because of their special magnetic properties and good biocompatibility. SPIONs can be manipulated by an external magnetic field to the anticipated site for desired bioimaging and therapy [111]. Inspired by this idea, several groups coupled UCNPs with SPIONs to form simultaneous multimodal imaging and targeted therapies. Shao and Liu et al. coupled UCNPs with SPIONs to form multifunctional nanoparticles (MFNPs) [112]. These MFNPs were further conjugated with folic acid to fabricate nanoprobes. The as-prepared MFNP nanoprobes were used for accurate targeting in UCL and MR imaging of FR-positive human epidermoid carcinoma KB cells and for molecular and magnetic targeted PTT of cancer cells. They successfully used PEGylated MFNPs for *in vitro* targeted UCL, MR, and dark-field imaging; for molecular and magnetic targeted PTT of HeLa cancer cells; and as a contrast agent for *in vivo* dual-modal UCL/MR imaging in KB tumor-bearing mice. The MFNPs based on UCNPs are promising tools for multimodality imaging, cell tracking, and imaging-guided novel targeted cancer therapy. Researchers further designed MFNPs with highly integrated UCL, superparamagnetism, and strong optical absorption capability. The MFNPs based on Au-shelled UCNP-SPION nanocomposites (hydrodynamic diameter of 220 nm) were constructed and applied for *in vivo* UCL/MR dual-modal imaging-guided magnetically targeted PDT. The MFNPs accumulated in tumors and exhibited excellent results in *in vivo* dual-modal optical/MR imaging of mice. Moreover, NIR irradiation induced 100% tumor elimination in a murine breast cancer model by Au PTT in MFNPs [113]

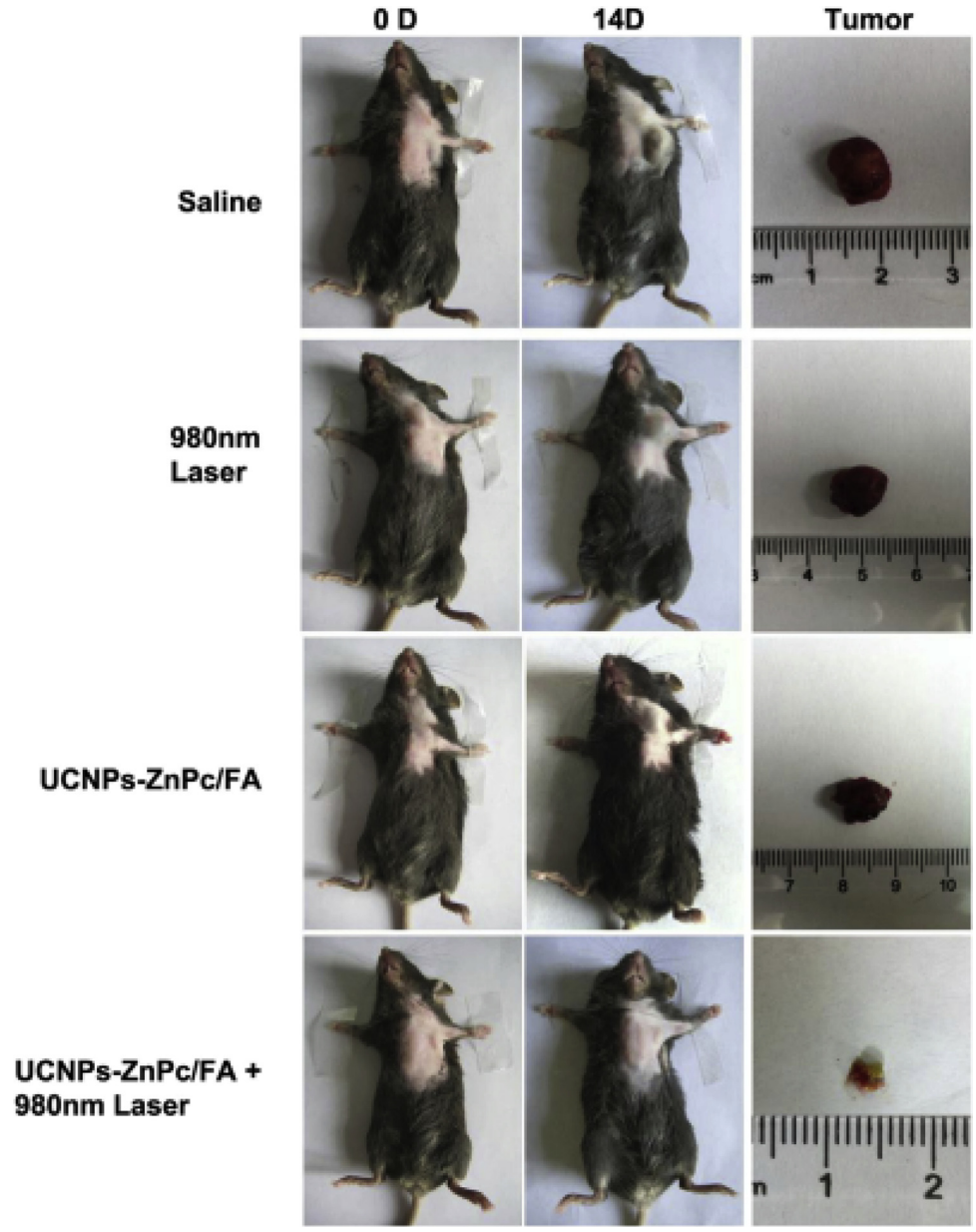

Fig. 11. Representative photos of mice and liver tumors before and after various treatments; photos of tumor tissue were obtained after 14 days. (Reprinted with permission from ref. [98]).

Silver is well-known to have strong plasmonic resonance performance. Song et al. prepared core-shell structured silver-coated $NaYF_4$:Yb,Er nanoparticles. PTT with synthesized UCNPs was conducted *in vitro* using HepG2 cells from human hepatic cancer and BCap-37 cells under 980-nm NIR light, and the optimum mortality approached 95% with a power density of 1.5 $W{\cdot}cm^{-2}$, which is much lower than that reported for Au nanoshells and Au nanorods [114]. Zhu and co-workers prepared the (Fig. 12)

carbon-coated core-shell upconversion nanocomposite $NaLuF_4$:Yb,Er@$NaLuF_4$@ Carbon (csUCNP@C, diameter of approximately 77 nm). They found the carbon shell was an excellent photothermal agent for cancer therapy and simultaneously heated the nanocomposite under 730-nm laser irradiation. This nanocomposite selectively killed HeLa cancer cells at a mild apparent temperature without harming adjacent cells (Fig. 13) [115]. Hyeon et al. prepared hexagonal-phase $NaYF_4$:Yb,Er/$NaGdF_4$ core–shell UCNPs conjugated to Ce6, which were used for both *in vivo* UCL/MRI dual-modal imaging and PDT for cancer. The obtained multifunctional material system enabled multimodal imaging and PDT for cancer [116]. Hu and collaborators prepared $NaYF_4$:Yb/Er@polypyrrole (PPy) core-shell nanoplates. The constructed nanoplates were an efficient PTT platform for *in vitro* and *in vivo* HeLa cancer cells guided simultaneously by CT imaging, UCL imaging, and infrared thermal imaging [117]. Their work provided a novel multimodal-imaging nanoplatform for imaging-guided cancer therapy. The fabrication of $LiYF_4$:Yb^{3+}/Tm^{3+}@SiO_2 UCNPs individually coated with a layer of chitosan hydrogel cross linked with a photocleavable crosslinker has drawn tremendous attention because these materials are excellent nanotransducers for converting longer visible (Vis) regions. This nanocomposite was also shown to be an excellent drug carrier, even under 2-cm thick tissue [118].

Kuang and co-workers constructed a plasmonic nanorod (NR) dimer-UCNP-Ce6 assembly for multimodal imaging-guided combination phototherapy. In this nanocomposite, the NR and UCNP were hierarchically engineered via DNA hybridization. *In vivo* experiments in mice showed that the nanocomposite accumulated in tumors through the enhanced permeability and retention effect and can

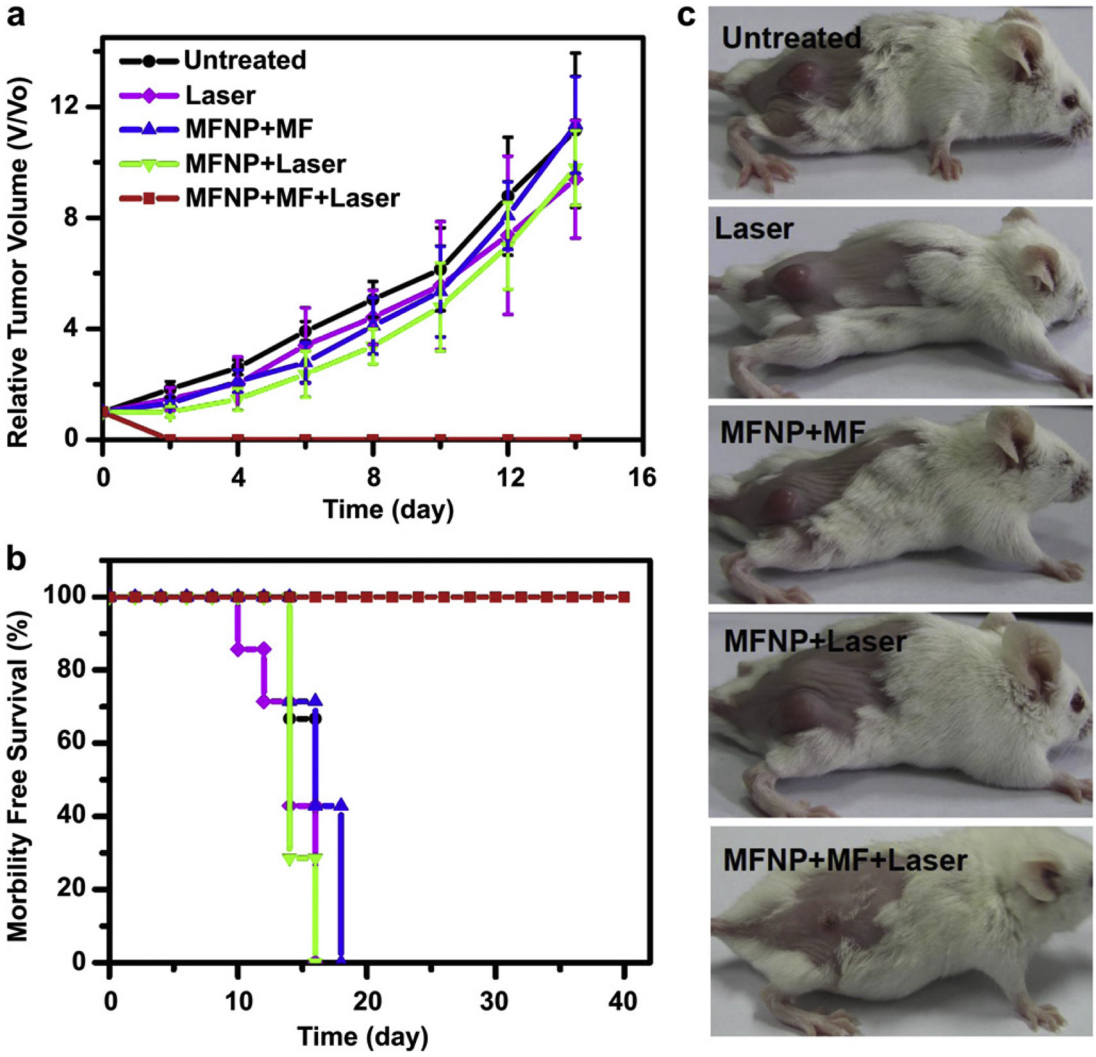

Fig. 12. *In vivo* magnetically targeted photothermal therapy. (a) Growth of 4T1 tumors in different groups of mice after treatment. Tumor volumes were normalized to their initial sizes. In the treatment group, 8 mice injected with MFNP-PEG were placed under a tumor-targeted magnetic field for 2 h and then exposed to an 808-nm laser at a power density of 1 W·cm^2 for 5 min. Four groups of mice (7 mice per group) were used as controls: (1) no MFNP injection and no laser (Untreated); (2) laser only without MFNP injection (Laser); (3) injected with MFNP under the magnetic field but without no laser irradiation (MFNP + MF); (4) injected with MFNP and exposed to the laser but without magnetic targeting (MFNP + Laser). Error bars show the SD. (b) Survival curves of mice bearing 4T1 tumors after various treatments indicated. MFNP-PEG injected mice with magnetic tumor-targeting after PTT treatment survived over 40 days with no deaths. (c) Representative photos of mice after various treatments indicated. (Reprinted with permission from ref. [113]).

serve as a multimodal agent for UCL, CT, PA, and MR imaging. Additionally, the nanocomposite, which can be switched on and off in the presence and absence of laser irradiation, was used with wavelength NIR light to shorter wavelengths spanning the UV range to the completely eliminate cervical cancer HeLa cells under NIR laser irradiation [119]. Xing and co-workers developed a new microenvironment-sensitive strategy for the localization of peptide-premodified UCNPs within tumor areas. Based on the tumor-specific cathepsin protease reaction, peptide cleavage induced covalent cross-linking between the exposed cysteine and 2-cyanobenzothiazole on neighboring particles, thus triggering the accumulation of UCNPs at the tumor site. The UCNPs exhibited strong tumor inhibition performance under 808-nm irradiation [120]. Lin et al. developed novel multifunctional GdOF:Ln@SiO_2 mesoporous capsules using UCL GdOF:Ln as cores and mesoporous silica layer as shells decorated with carbon dots ($Gd(OH)_x(CO_3)_yF_z$:Ln@C@SiO_2, approximately 280 nm in width and 500 nm in length), conjugated with ZnPc and doxorubicin (DOX). The system was endowed with excellent UCL imaging, MRI, and CT imaging properties and killed cancer cells (Fig. 14) [121]. Therefore, the UCNP nanoplatform is a powerful tool for treating cancer cells.

8. Drug delivery based on UCNPs

UCNPs can deliver drugs to the targeted tumor site for drug release and disease treatment. In this process, UCNPs can also be used for tracer imaging to evaluate the efficiency and distribution of drug release and examine related mechanisms, among other functions. Therefore, UCNPs as a drug carrier in the diagnosis and treatment of major diseases has broad application prospects. Nearly all drug delivery systems involving UCNPs are based on physical adsorption and chemical bond for loading drugs. The UCNP surface is mostly coated with PEG or modified mesoporous silica to improve biocompatibility [122,123]. UCNPs with specific upconverted emission wavelengths can double as a photon-transducer to activate the photosensitizer for payload-carried drugs triggered by NIR light in deep tissue [124]. For site-specific drug delivery, drug-carriers with an acceptor molecule that specifically recognize a receptor on the surface of target cells have been widely studied. Such target-specific recognition includes antigen-antibody and ligand-acceptor interactions, providing an effective approach for precision medicine for treating cancer with a lower health-care cost and better treatment outcomes [125,126].

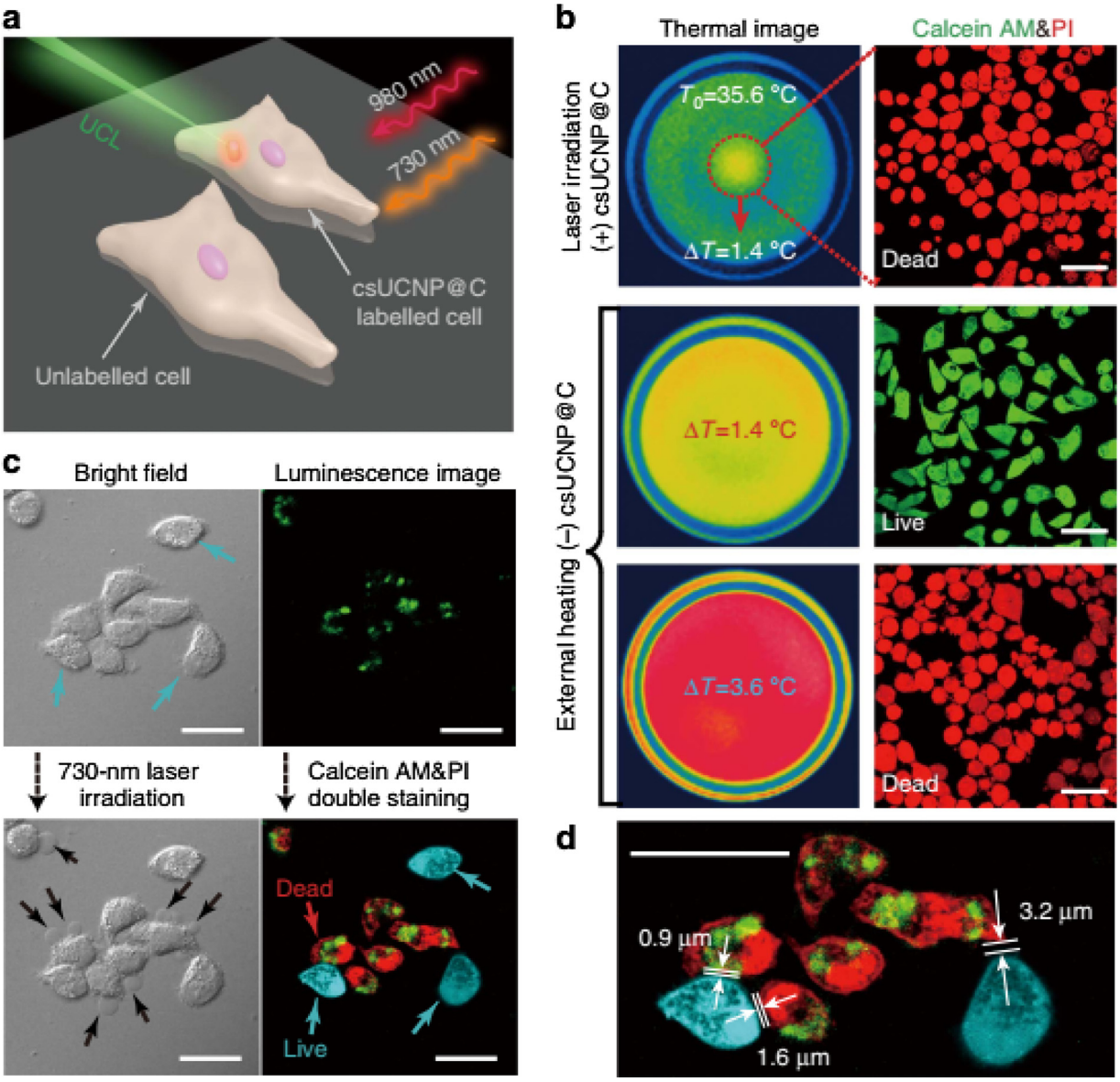

Fig. 13. csUCNP@C for high-accuracy PTT at the cell level. (a) Schematic diagram of PTT in cells. (b) Thermal images and Calcein AM and PI double-stained images of HeLa cells treated with photothermal ablation or external heating. Non-labeled cells were irradiated by 730 nm laser (0.3 W·cm^{-2}) and the final apparent temperature elevation in the laser spot (T_0 = 35.6 °C) was set as a benchmark. △T is the difference between the apparent temperature and T_0. In external heating, cells were alive when △T = 1.4 °C and dead when △T = 3.6 °C. At 730-nm laser irradiation, csUCNP@C-labeled cells were dead when △T = 1.4 °C, indicating that the eigen temperature of csUCNP@C had reached a lethal temperature to the cells although the apparent temperature was still safe. Scale bar, 50 μm. (c) Photothermal therapy of HeLa cells under 730-nm laser irradiation at 0.3 W.cm^{-2} for 5 min. Cells labeled with csUCNP@C showed a strong UCL signal in the cytoplasm (green). The signal is detected in the wavelength region of 520–550 nm. After 730 nm irradiation, dead cells showed conspicuous cytoplasm leakage, which is labeled with black arrows. Calcein AM (cyan) and PI (red) double-staining showed that only the cells labeled with csUCNP@C were dead. Scale bar, 30 μm. (d) Amplified image of the luminescent cell images in c. The distance between the adjacent live and dead cells was measured. The minimum distance was ˜0.9 μm. Scale bar, 30 μm. (Reprinted with permission from ref. [115]).

UCNPs have a large surface area, unique structures, and versatile surface chemistries. Therefore, they can serve as nanocarriers for drug delivery and upconverted luminescent nanoprobes [127]. Lin and his group synthesized core-shell structured mesoporous-silica-coated up-conversion Gd_2O_3:Er^{3+} particles. The nanocomposite released green upconversion emission under 980-nm NIR excitation and showed controlled drug-release of ibuprofen [128]. Bu and co-workers prepared UCNPs ($NaYF_4$:Yb/Tm@$NaGdF_4$) embedded in the core of hollow mesoporous silica nanoparticles (diameter of approximately 70 nm) as a carrier of the anticancer drug DOX. The nanosensors were used to visualize and quantify drug release by simultaneously monitoring UCL and T_1-MRI in real-time. This nanosensor provided a useful tool for controlling the dosage of anticancer drugs in the clinic (Fig. 15) [129].

Liu and co-workers first functionalized UCNPs with a PEG-grafted amphiphilic polymer. The PEGylated UCNPs were loaded with DOX through physical adsorption for intracellular drug delivery. The UCNP nanocomposites were further conjugated with folic acid. Their analysis demonstrated that multi-functional UCNPs could selectively target, effectively label, and release drugs to human nasopharyngeal epidermal carcinoma KB cells [130]. Lin and his collaborators developed a multifunctional nanocomposite combining UCL/MR/CT tri-modality imaging and NIR-activated platinum pro-drug delivery together using UCNPs as nanotransducers. Under 980-nm irradiation, the nanocomposite not only effectively killed cancer cells but also functioned as

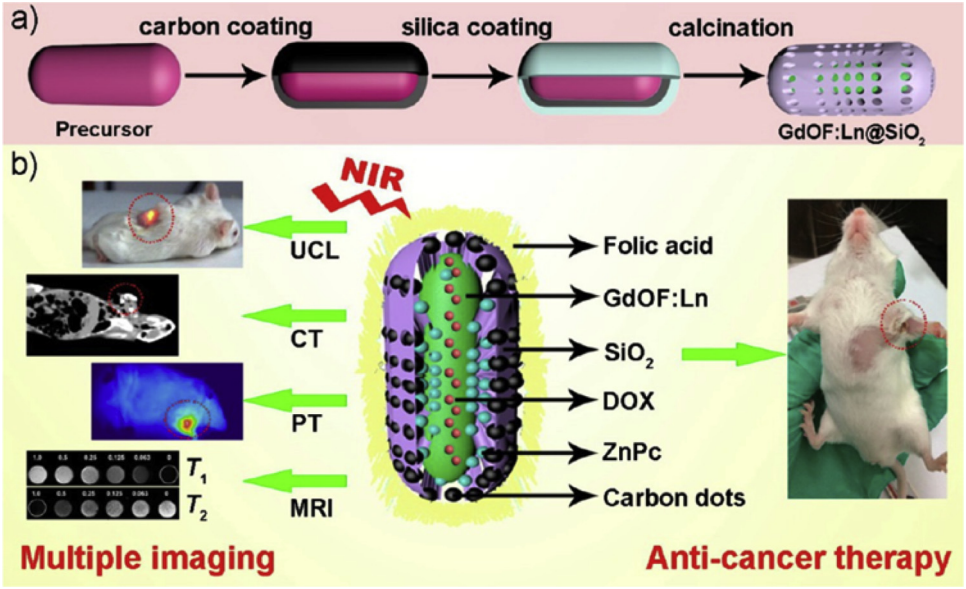

Fig. 14. Schematic illustration of the synthesis of GdOF:Ln@SiO_2-ZnPc-CDs microcapsules and bio-application for multiple imaging and anti-tumor therapy (Reprinted with permission from ref. [121]. Copyright 2015 American Chemical Society).

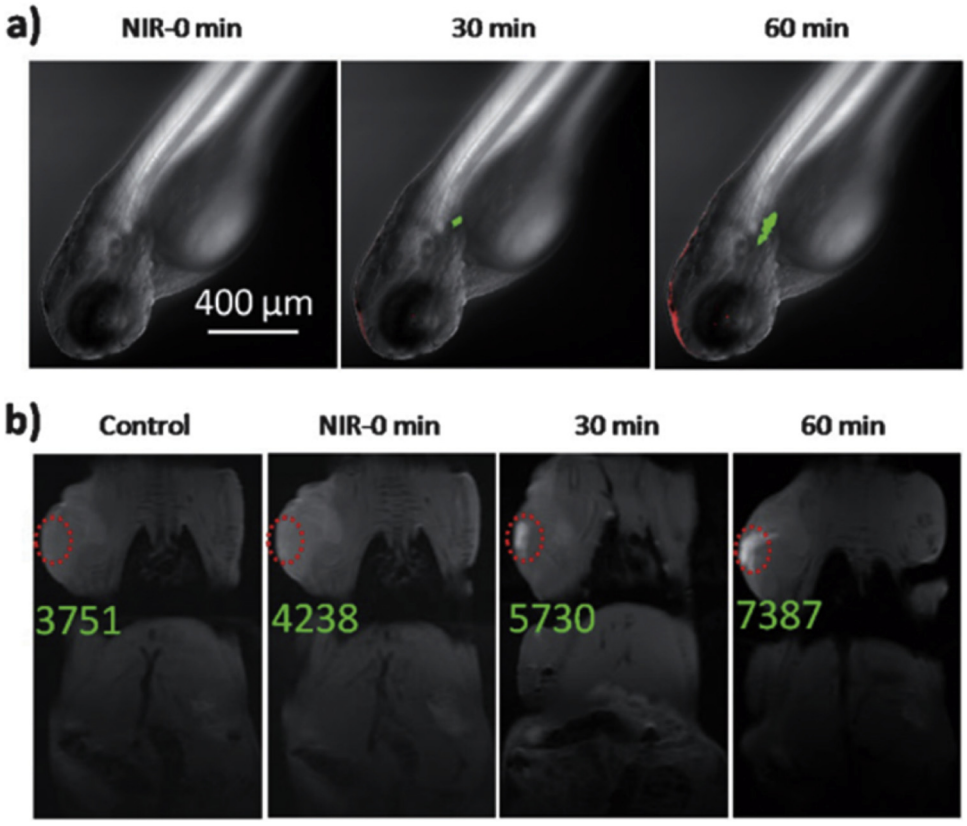

Fig. 15. a) Confocal laser scanning microscopy images of zebrafish, in which UCNP signals are green and DOX signals are red. All images share the same scale bar (400 μm). b) T1-MR images of a Walker 256 tumor-bearing Sprague Dawley rat injected with nanosensor 2 (1 mg mL^{-1}, 100 μL) subcutaneously before and after NIR exposure for different times (n = 3). The red circles indicate the tumor area where nanosensor 2 was injected. The T1-MR signal intensities before and after NIR exposure are also shown in the figures. The power density of NIR light employed was 1.5 W·cm^{-2} (Reprinted with permission from ref. [129]).

excellent contrast agents for UCL/MR/CT tri-modality imaging, and thus can provide complete information for cancer diagnosis and therapy [131]. They also fabricated a multifunctional nanocomposite based on UCNPs that served as an anti-cancer drug carrier of cisplatin (IV) and *in vitro/in vivo* imaging. The nanocomposites can be used as luminescent nanoprobes for UCL *in vitro/in vivo* imaging. Cisplatin (IV) effectively promotes the apoptosis of tumor cells [132]. Park and his team synthesized core-shell nanoparticles composed of UCNP as a core and a graphene oxide quantum dot. Hypocrellin A was further loaded onto the graphene oxide quantum dots through π-π stacking for PDT. The fabricated system was used to not only image and damage cervical cancer HeLa cells, but also to carry the antitumor drug hypocrellin A to the desired site [133].

The development of a multi-functional UCNP nanoplatform that integrates cancer diagnosis and treatment with a low level of side effects is a research hotspot in the field of nano-oncology. Dan et al. prepared the nano-system MIL-100 (Fe) with metal-organic framework-coated $NaGdF_4$:Yb,Tm@$NaGdF_4$:Yb,Nd UCNPs (diameter of approximately 30 nm). Under 808-nm laser irradiation, this nanosystem produced large amounts of ROS, which killed cancer cells. At the same

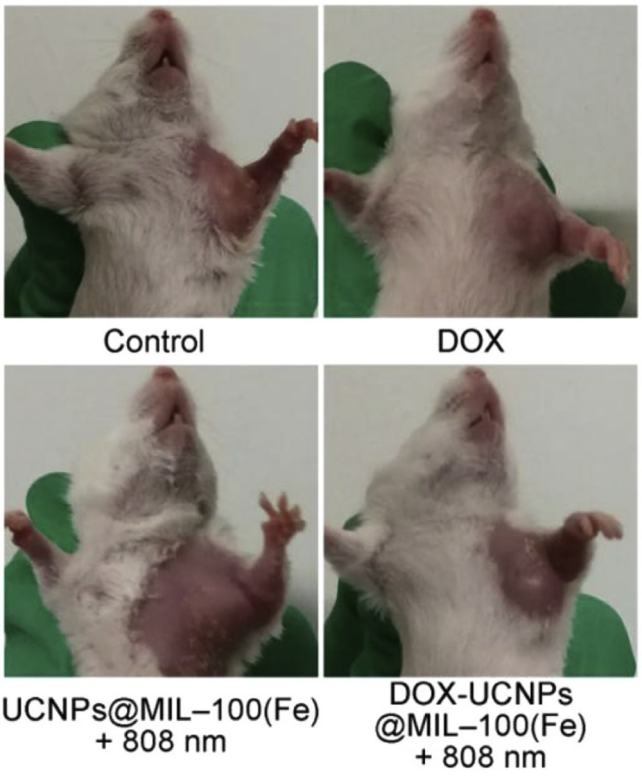

Fig. 16. Representative photographs of tumor-bearing mice treated with normal saline, pure DOX, UCNPs@MIL-100(Fe) NPs with 808-nm laser irradiation (0.5 W·cm^2) for 5 min, and DOXUCNPs@MIL-100(Fe) NPs with 808-nm laser irradiation (0.5 W·cm^2) for 5 min (0.1 mL, 500 μg mL) on the 14th day. (Reprinted with permission from ref. [134]).

time, MIL-100 (Fe) can convert laser radiation into heat, thus achieving the effect of PTT treatment. Moreover, MIL-100 (Fe) has a porous structure and can be loaded with a large amount of DOX. It has been demonstrated both *in vivo* and *in vitro* that UCNPs@MIL-100(Fe) nanoparticles loaded with DOX significantly inhibit the growth of cancer cells under 808-nm laser irradiation (0.5 W·m^2) based on synergistic PDT, PTT, and chemotherapy effects (Fig. 16) [134].

To date, numerous carriers of anticancer drugs based on UCNPs have been studied. Most of these carriers exhibited great advantages, such as a high efficiency, low toxicity, and few side effects [135,136]. These studies provided a new approach for targeted drug delivery with low side effects and real-time monitoring of anticancer drug release.

9. Prospects and challenges

This review presents a brief survey of the latest advances in UCNP-based cancer diagnosis and therapy. As a promising nanomaterial, UCNPs can be excited by light in the NIR region and emit fluorescence while evading the autofluorescence induced by biological tissue. Moreover, the excitation light of UCNPs can deeply penetrate the tissue as well as living organisms. UCNPs are a versatile platform as an excellent multimodal imaging nanocomposite for cancer and outstanding drug carrier for chemotherapy. Additionally, as a multifunctional nanoplatform, UCNPs can be used in PDT and PTT of cancer.

Despite these exciting advancements, additional studies are needed before UCNPs can be clinically applied. First, UCNPs with high UCL quantum yield nanomaterials must be acquired. The UCNPs show excellent advantages, including low toxicity, long life, large anti-Stokes displacement, large penetration depth, and strong resistance to light corrosion and matte flicker. As a result, these materials offer unique advantages for imaging, long-distance communication, biomarkers, lasers, and security tags. However, the widely studied $NaYF_4$-doped Yb^{3+} and Er^{3+} UCNPs, which are as the most efficient UCNPs, have a quantum yield of only 0.005–0.3% [137,138]. Therefore, new UCNPs and synthetic methods are needed to obtain UCNPs with smaller particle sizes and greater uniformity, excellent biocompatibility, and high fluorescence quantum yield. Biosafety is another concern. Although numerous studies have demonstrated that UCNPs are safe in the short-term *in vitro* and *in vivo*, the long-term toxicity and potential accumulation of UCNPs are not well-understood. Additionally, the interaction of UCNPs with the immune system and reproductive system is largely unexplored. Studies are also needed to decrease potential photodamage. Using the current UCNP system, 980-nm NIR light is generally used as the laser source. However, the main limitation of 980-nm excitation for *in vivo* application is the overheating effect. Therefore, a method using another excitation source in the NIR region rather than 980 nm may decrease the overheating effects of the laser source. As multifunctional agents, UCNPs are not only good contrast agents, but are also excellent drug carriers for cancer. Although some combination formulations have been successfully developed and showed satisfactory outcomes, studies of UCNP-based cancer diagnosis and therapy multifunction are still in the early stages. Studies are also needed to explore and discover cancer molecular markers with high sensitivity and specificity. The discovery of sensitive and specific cancer molecular markers will facilitate the development of highly efficient and specific UCNP nanoprobes for cancer.

Many innovative studies are needed in this emerging field. Once the limitations listed above are resolved, UCNPs can be used for accurate detection and effective treatment of cancer, enabling the development of new methods for diagnosing and treating cancers during early stages in the clinic.

Ethics approval and consent to participate

Not applicable.

Consent for publication

Not applicable.

Availability of data and materials

Not applicable,

Competing interests

The authors declare that they have no competing interests.

Authors' contributions

Kunmeng Li, Enlv Hong, Bing Wang and Zhiyu Wang carried out the literature collection and classification, writing, and revising the manuscript; Liwen Zhang and Ruixia Hu, carried out the literature collection and classification, writing, and participated in the sequence alignment. Dr. Baiqi Wang conceived the study, participated in its design and coordination, and helped to draft and revise the manuscript. All authors read and approved the final manuscript.

Authors' information

Dr. Baiqi Wang is an associate professor at the Department of Occupational and Environmental Health of Tianjin Medical University (TMU) of China. He received his PhD in Applied Chemistry from Harbin Institute of Technology in 2006. Next, he worked as a postdoctoral fellow at the State Key Laboratory for Artificial Microstructure and Mesoscopic Physics in Peking University. After two years, he joined TMU as faculty. In 2013, he worked in the School of Medicine of the Johns Hopkins University as a visiting scholar. His research interests include synthesis, modification of new functionalized nanomaterials,

and their applications in the cancer detection and treatment fields. To date, Dr. Wang has published more than 40 peer-reviewed articles.

Acknowledgments

This work was financially supported by The Open Project of The Key Laboratory of Modern Toxicology of Ministry of Education, Nanjing Medical University (NMUAMT201808); Natural Sciences Foundation of Tianjin City of China (No. 12JCYBJC19100); and Fujian Natural Science Fund Project (2017J01301).

References

[1] D. Hanahan, R.A. Weinberg, The hallmarks of cancer, Cell 100 (2000) 57–70.
[2] R.L. Siegel, K.D. Miller, Jemal A. Cancer Statistics, CA Cancer J. Clin. (68) (2018) 7–30 2018.
[3] American Cancer Society, http://www.cancer.org/cancer/breastcancer/detailedguide/breast-cancer-survival-by-stage.
[4] N. Bertrand, J. Wu, X.Y. Xu, N. Kamaly, O.C. Farokhzad, Cancer nanotechnology: the impact of passive and active targeting in the era of modern cancer biology, Adv. Drug Deliv. Rev. 66 (2014) 2–25.
[5] M. Ferrari, Cancer nanotechnology: opportunities and challenge, Nat. Rev. Cancer 5 (2005) 161–171.
[6] X.D. Wang, R.R. Vallev, T.Y. Ohulchanskyy, H. Agren, C.H. Yang, G.Y. Chen, Dye-sensitized lanthanide-doped upconversion nanoparticles, Chem. Soc. Rev. 46 (2017) 4150–4167.
[7] W.P. Fan, W.B. Bu, J.L. Shi, On the latest three-stage development of nanomedicines based on upconversion nanoparticles, Adv. Mater. 28 (2016) 3987–4011.
[8] M. Wang, G. Abbineni, A. Clevenger, C. Mao, S. Xu, Upconversion nanoparticles: synthesis, surface modification, and biological applications, Nanomedicine 7 (2011) 710–729.
[9] F. Auzel, Upconversion and anti-stokes processes with f and d ions in solids, Chem. Rev. 104 (2004) 139–174.
[10] S. Han, R. Deng, X. Xie, Enhancing luminescence in lanthanide-doped upconversion nanoparticles, Angew. Chem. Int. Ed. 53 (2014) 11702–11715.
[11] L.D. Sun, Y.F. Wang, C.H. Yan, Paradigms and challenges for bioapplication of rare earth upconversion luminescent nanoparticles: small size and tunable emission/excitation spectra, Acc. Chem. Res. 47 (2014) 1001–1009.
[12] X. Li, F. Zhang, D. Zhao, Lab on upconversion nanoparticles: optical properties and applications engineering via designed nanostructure, Chem. Soc. Rev. (2014), https://doi.org/10.1039/c4cs00163j.
[13] B. Zhou, D.Y. Shi Jin, et al., Controlling upconversion nanocrystals for emerging applications, Nat. Nanotechnol. 10 (2015) 925–936.
[14] J. Shen, L. Zhao, Han Gang, Lanthanide-doped upconverting luminescent nanoparticle platforms for optical imaging-guided drug delivery and therapy, Adv. Drug Deliv. Rev. 65 (2013) 744–755.
[15] T.M. Liu, J. Conde, T. Lipinski, et al., Smart NIR linear and nonlinear optical nanomaterials for cancer theranostics: prospects in photomedicine, Prog. Mater. Sci. 88 (2017) 89–135.
[16] S.L. Wang, A.Y. Bi, W.B. Zeng, et al., Upconversion nanocomposites for photo-based cancer theranostics, J. Mater. Chem. B Mater. Biol. Med. 4 (2016) 5331–5348.
[17] A.R. Miandashti, M.E. Kordesch, H.H. Richardson, et al., Effect of temperature and gold nanoparticle interaction on the lifetime and luminescence of NaYF4:Yb^{3+}:Er^{3+} upconverting nanoparticles, ACS Photon. 4 (2017) 1864–1869.
[18] D.Y. Jin, P. Xi, B.M. Wang, et al., Nanoparticles for super-resolution microscopy and single-molecule tracking, Nat. Methods 15 (2018) 415–423.
[19] P. Li, Y. Yan, B.L. Chen, et al., Lanthanide-doped upconversion nanoparticles complexed with nano-oxide graphene used for upconversion fluorescence imaging and photothermal therapy, Biomater. Sci. 6 (2018) 877-844.
[20] Z.X. Meng, L.P. Zhang, Z.G. He, et al., Mucosal penetrating bioconjugate coated upconverting nanoparticles that integrate biological tracking and photodynamic therapy for gastrointestinal cancer treatment, ACS Biomater. Sci. Eng. 4 (2018) 2203–2212.
[21] H.L. Li, W.Y. Lei, J.N. Wu, et al., An upconverting nanotheranostic agent activated by hypoxia combined with NIR irradiation for selective hypoxia imaging and tumour therapy, J. Mater. Chem. B Mater. Biol. Med. 6 (2018) 2747–2757.
[22] L. Chunxia, X. Lili, L. Zihua, et al., Current progress on the controlled synthesis and biomedical applications of ultrasmall (< 10 nm) $NaREF_4$ nanoparticles, Dalton Trans. (2018), https://doi.org/10.1039/C8DT00258D.
[23] L. Labrador-Paez, E.C. Ximendes, P. Rodriguez-Sevilla, et al., Core-shell rare-earth-doped nanostructures in biomedicine, Nanoscale 10 (2018) 12935–12956.
[24] C.L. Yan, H.Z. Zhao, D.F. Perepichka, F. Rosei, Lanthanide ion doped upconverting nanoparticles: synthesis, structure and properties, Small 12 (2016) 3888–3907.
[25] C. Liang, W. Chao, L. Zhuang, Upconversion nanoparticles and their composite nanostructures for biomedical imaging and cancer therapy, Nanoscale 5 (2013) 23.
[26] T. Gan, Z. Xiao, G. Zhanjun, Y. Zhao, Recent advances in upconversion nanoparticles-based multifunctional nanocomposites for combined cancer therapy, Adv. Mater. 27 (2015) 7692–7712.
[27] Y. Dongmei, L. Chunxia, L. Jun, Multimodal cancer imaging using lanthanide-based upconversion nanoparticles, Nanomedicine 10 (2015) 2573–2591.
[28] L. Yuan, W.Y. Lin, K.B. Zheng, S.S. Zhu, FRET-based small-molecule fluorescent probes: rational design and bioimaging applications, Acc. Chem. Res. 46 (2013) 1462–1473.
[29] J.D. Wang, F.J. Cao, S.J. He, Y. Xia, X.Y. Liu, W.X. Jiang, Zhang H.S. Yu YY, W.W. Chen, FRET on lateral flow test strip to enhance sensitivity for detecting cancer biomarker, Talanta 176 (2018) 444–449.
[30] Z.Q. Li, Y. Zhang, S. Jiang, Multicolor core/shell-Structured upconversion fluorescent nanoparticles, Adv. Mater. 20 (2008) 4765–4769.
[31] Q.Q. Wu, H.Y. Chen, A.J. Fang, X.Y. Wu, M.L. Liu, H.T. Li, Y.Y. Zhang, S.Z. Yao, Universal multifunctional nanoplatform based on target-induced in situ promoting Au seeds growth to quench fluorescence of upconversion nanoparticles, ACS Sens. 2 (2017) 1805–1813.
[32] L. Wang, R. Yan, Z. Huo, et al., Fluorescence resonant energy transfer biosensor based on upconversion-luminescent nanoparticles, Angew. Chem. Int. Ed. 44 (2005) 6054–6057.
[33] H.J. Zijlmans, J. Bonnet, J. Burton, et al., Detection of cell and tissue surface antigens using up-converting phosphors: a new reporter technology, Anal. Biochem. 267 (1999) 30–36.
[34] M. Wang, W. Hou, C. Mi, et al., Immunoassay of goat antihuman immunoglobulin G antibody based on luminescence resonance energy transfer between near-Infrared responsive $NaYF_4$:Yb, Er upconversion fluorescent nanoparticles and gold nanoparticles, Anal. Chem. 81 (2009) 8783–8789.
[35] C. Zhang, Y. Yuan, S. Zhang, et al., Biosensing platform based on fluorescence resonance energy transfer from upconverting nanocrystals to graphene oxide, Angew. Chemie Int. Ed. English 50 (2011) 6851–6854.
[36] M. Lin, Y. Gao, T.J. Diefenbach, et al., Facial layer-by-layer engineering of up-conversion nanoparticles for gene delivery: near-infrared-initiated fluorescence resonance energy transfer tracking and overcoming drug resistance in ovarian Cancer, ACS Appl. Mater. Interfaces 9 (2017) 7941–7949.
[37] S. Li, L. Xu, W. Ma, et al., Dual-mode ultrasensitive quantification of MicroRNA in living cells by chiroplasmonic nanopyramids self-assembled from gold and up-conversion nanoparticles, J. Am. Chem. Soc. 138 (2016) 306–312.
[38] B. Gu, Y. Zhou, X. Zhang, et al., Thiazole derivative-modified upconversion nanoparticles for Hg^{2+} detection in living cells, Nanoscale 8 (2016) 276–282.
[39] R. Wei, Z. Wei, L. Sun, et al., Nile red derivative-modified nanostructure for up-conversion luminescence sensing and intracellular detection of Fe^{3+} and MR imaging, ACS Appl. Mater. Interfaces 8 (2016) 400–410.
[40] T. Liang, Z. Li, D. Song, et al., Modulating the luminescence of upconversion nanoparticles with heavy metal ions: a new strategy for probe design, Anal. Chem. 88 (2016) 9989–9995.
[41] F. Van de Rijke, H. Zijlmans, S. Li, et al., Up-converting phosphor reporters for nucleic acid microarrays, Nat. Biotechnol. 19 (2001) 273–276.
[42] P. Corstjens, M. Zuiderwijk, A. Brink, et al., Use of up-converting phosphor reporters in lateral-flow assays to detect specific nucleic acid sequences: a rapid, sensitive DNA test to identify human papillomavirus type 16 infection, Clin. Chem. 47 (2001) 1885–1893.
[43] J. Liu, L. Lu, A. Li, et al., Simultaneous detection of hydrogen peroxide and glucose in human serum with upconversion luminescence, Biosens. Bioelectron. 68 (2015) 204–209.
[44] J. Hampl, M. Hall, N.A. Mufti, et al., Upconverting phosphor reporters in Immunochromato- graphic assays, Anal. Biochem. 288 (2001) 176–187.
[45] L. Xun, Shang-Qing Zhang, W. Xing, et al., A novel “modularized” optical sensor for pH monitoring in biological matrixes, Biosens. Bioelectron. (2018), https://doi.org/10.1016/j.bios.2018.02.052.
[46] W. Zheng, S. Zhou, Z. Chen, et al., Sub-10 nm lanthanide-doped CaF_2 nanoprobes for time-resolved luminescent biodetection, Angew. Chemie Int. Ed. English 52 (2013) 6671–6676.
[47] Z. Chen, W. Zheng, P. Huang, et al., Lanthanide-doped luminescent nano-bioprobes for the detection of tumor markers, Nanoscale 7 (2015) 4274–4290.
[48] P. Vilela, A. El-Sagheer, T.M. Millar, et al., Graphene oxide-upconversion nanoparticle based optical sensors for targeted detection of mRNA biomarkers present in alzheimer’s disease and prostate cancer, ACS Sens. 2 (2017) 52–56.
[49] A. Fang, H. Chen, H. Li, et al., Glutathione regulation-based dual-functional up-conversion sensing platform for acetylcholinesterase activity and cadmium ions, Biosens. Bioelectron. 87 (2017) 545–551.
[50] R.A. Jalil, Y. Zhang, Biocompatibility of silica coated $NaYF_4$ upconversion fluorescent nanocrystals, Biomaterials 29 (2008) 4122–4128.
[51] N.M. Idris, Z. Li, L. Ye, et al., Tracking transplanted cells in live animal using upconversion fluorescent nanoparticles, Biomaterials 30 (2009) 5104–5113.
[52] Z. Gu, L. Yan, G. Tian, et al., Recent advances in design and fabrication of up-conversion nanoparticles and their safe theranostic applications, Adv. Mater. 25 (2013) 3758–3779.
[53] H.H. Gorris, O.S. Wolfbeis, Photon-upconverting nanoparticles for optical encoding and multiplexing of cells, biomolecules, and microspheres, Angew. Chemie Int. Ed. English 52 (2013) 2–19.
[54] S.F. Lim, R. Riehn, W.S. Ryu, et al., In vivo and scanning Electron microscopy imaging of upconverting nanophosphors in Caenorhabditis elegans, Nano Lett. 6 (2006) 169–174.
[55] P. Zhang, W. Steelant, M. Kumar, et al., Versatile photosensitizers for photodynamic therapy at infrared excitation, J. Am. Chem. Soc. 129 (2007) 4526–4527.
[56] D.K. Chatterjee, A.J. Rufaihanh, Y. Zhang, Upconversion fluorescence imaging of cells and small animals using lanthanide doped nanocrystals, Biomaterials 29 (2008) 937–943.
[57] M. Nyk, R. Kumar, T.Y. Ohulchanskyy, et al., High contrast in vitro and in vivo photoluminescence bioimaging using near infrared to near infrared up-conversion in Tm^{3+} and Yb^{3+} doped fluoride nanophosphors, Nano Lett. 8 (2008)

3834–3838.
[58] Y. Ma, Y. Ji, M. You, et al., Labeling and long-term tracking of bone marrow mesenchymal stem cells in vitro using $NaYF_4$:Yb^{3+},Er^{3+} upconversion nanoparticles, Acta Biomater. 42 (2016) 199–208.
[59] L. Zhao, A. Kutikov, J. Shen, et al., Stem cell labeling using polyethylenimine conjugated (α-$NaYbF_4$:Tm^{3+})/CaF_2 upconversion nanoparticles, Theranostics 3 (2013) 249–257.
[60] J. Li, W.Y. Lee, T. Wu, et al., Near-infrared light-triggered release of small molecules for controlled differentiation and long-term tracking of stem cells in vivo using upconversion nanoparticles, Biomaterials 110 (2016) 1–10.
[61] C. Wang, L. Cheng, H. Xu, et al., Towards whole-body imaging at the single cell level using ultra-sensitive stem cell labeling with oligo-arginine modified upconversion nanoparticles, Biomaterials 23 (2012) 4872–4881.
[62] L. Xiong, Z. Chen, Q. Tian, et al., High contrast upconversion luminescence targeted imaging in vivo using peptide-labeled nanophosphors, Anal. Chem. 81 (2009) 8687–8694.
[63] L. Xiong, Z. Chen, M. Yu, et al., Synthesis, characterization, and in vivo targeted imaging of amine-functionalized rare-earth up-converting nanophosphors, Biomaterials 30 (2009) 5592–5600.
[64] X. Yu, Z. Sun, M. Li, et al., Neurotoxin-conjugated upconversion nanoprobes for direct visualization of tumors under near-infrared irradiation, Biomaterials 31 (2010) 8724–8731.
[65] M. Wang, C. Mi, W. Wang, et al., Immunolabeling and NIR-excited fluorescent imaging of HeLa cells by using $NaYF_4$:Yb,Er upconversion nanoparticles, ACS Nano 3 (2009) 1580–1586.
[66] Y. Shi, B. Shi, A.V.E. Dass, et al., Stable upconversion nanohybrid particles for specifc prostate Cancer cell immunodetection, Sci. Rep. 6 (2016) 37533.
[67] C. Mi, Z. Tian, C. Cao, et al., Novel Microwave-Assisted Solvothermal Synthesis of $NaYF_4$: Yb,Er Upconversion Nanoparticles and Their Application in Cancer Cell Imaging, Langmuir 27 (2011) 14632–14637.
[68] J.C. Boyer, M.P. Manseau, J.I. Murray, et al., Surface modification of upconverting $NaYF_4$ nanoparticles with PEG-Phosphate ligands for NIR (800 nm) biolabeling within the biological window, Langmuir 26 (2010) 1157–1164.
[69] L. Rao, L. Bu, B. Cai, et al., Cancer cell membrane-coated upconversion nanoprobes for highly specific tumor imaging, Adv. Mater. 28 (2016) 3460–3466.
[70] C. Liu, Y. Qi, R. Qiao, et al., Detection of early primary colorectal Cancer with upconversion luminescence NPs-based molecular probes, Nanoscale 8 (2016) 12579–12587.
[71] Y.I. Park, J.H. Kim, K.T. Lee, et al., Nonblinking and nonbleaching upconverting nanoparticles as an optical imaging nanoprobe and T1 magnetic resonance imaging contrast agent, Adv. Mater. 21 (2009) 4467–4471.
[72] J. Zhou, Y. Sun, X. Du, et al., Dual-modality in vivo imaging using rare-earth nanocrystals with near-infrared to near-infrared (NIR-to-NIR) upconversion luminescence and magnetic resonance properties, Biomaterials 31 (2010) 3287–3295.
[73] J. Zhou, M. Yu, Y. Sun, et al., Fluorine-18-labeled Gd^{3+}/Yb^{3+}/Er^{3+} co-doped $NaYF_4$ nanophosphors for multimodality PET/MR/UCL imaging, Biomaterials 32 (2011) 1148–1156.
[74] R. Kumar, M. Nyk, T.Y. Ohulchanskyy, et al., Combined optical and MR bioimaging using rare earth ion doped $NaYF_4$ nanocrystals, Adv. Funct. Mater. 19 (2009) 853–859.
[75] G. Chen, T.Y. Ohulchanskyy, W.C. Law, et al., Monodisperse $NaYbF_4$:Tm^{3+}/$NaGdF_4$ core/shell nanocrystals with nearinfrared to near-infrared upconversion photoluminescence and magnetic resonance properties, Nanoscale 3 (2011) 2003–2008.
[76] A. Xia, Y. Gao, J. Zhou, et al., Core–shell $NaYF_4$:Yb^{3+},Tm^{3+}@Fe_xO_y nanocrystals for dual-modality T2-enhanced magnetic resonance and NIR-to-NIR upconversion luminescent imaging of small-animal lymphatic node, Biomaterials 32 (2011) 7200–7208.
[77] L. Rao, W. Lu, T. Zeng, et al., Sub-10 nm $BaLaF_5$: Mn/Yb/Er nanoprobes for dual-modal synergistic in vivo upconversion luminescence and X-ray bioimaging, J. Mater. Chem. B Mater. Biol. Med. 2 (2014) 6527–6533.
[78] F. Chen, S. Zhang, W. Bu, et al., A "Neck-Formation" strategy for an antiquenching Magnetic/Upconversion fluorescent dual-modal cancer probe, Chem. Eur. J. 16 (2010) 11254–11260.
[79] Y. Sun, M. Yu, S. Liang, et al., Fluorine-18 labeled rare-earth nanoparticles for positron emission tomography (PET) imaging of sentinel lymph node, Biomaterials 32 (2011) 2999–3007.
[80] Y. Yang, Y. Sun, T. Cao, et al., Hydrothermal synthesis of $NaLuF_4$:^{153}Sm,Yb,Tm nanoparticles and their application in dual-modality upconversion luminescence and SPECT bioimaging, Biomaterials 34 (2013) 774–783.
[81] Zhou X, Chen J, M. Chen, et al., Core–shell Fe_3O_4@$NaLuF_4$:Yb,Er/Tm nanostructure for MRI, CT and upconversion luminescence tri-modality imaging, Biomaterials 33 (2012) 4618–4627.
[82] Q. Liu, Y. Sun, C. Li, et al., 18F-labeled magnetic-upconversion nanophosphors via rare-earth cation-assisted ligand assembly, ACS Nano 5 (2011) 3146–3157.
[83] D. Hongling, H. Sa, X. Chen, Intensely red-emitting luminescent upconversion nanoparticles for deep-tissue multimodal bioimaging, Talanta 184 (2018) 461–467.
[84] N. Kang, Y. Liu, Y. Zhou, et al., Phase and size control of core–Shell upconversion nanocrystals light up deep dual luminescence imaging and CT in vivo, Adv. Healthc. Mater. 5 (2016) 1356–1363.
[85] W. Yuan, D. Yang, Q. Su, et al., Intraperitoneal administration of biointerface-camouflaged upconversion nanoparticles for contrast enhanced imaging of pancreatic cancer, Adv. Funct. Mater. 26 (2016) 8631–8642.
[86] Z. Xue, Z. Yi, X. Li, et al., Upconversion optical/magnetic resonance imaging-guided small tumor detection and in vivo tri-modal bioimaging based on high-performance luminescent nanorods, Biomaterials 115 (2017) 90–103.
[87] W. Yuan, L. Dan, Z. Fang, et al., Versatile in-situ synthesis of MnO_2 nanolayers on upconverting nanoparticles and application for activatable fluorescence and MRI imaging, Chem. Sci. (2018), https://doi.org/10.1039/C8SC00490K.
[88] J. Zhou, Z. Liu, F. Li, Upconversion nanophosphors for small-animal imaging, Chem. Soc. Rev. 41 (2012) 1323–1349.
[89] X. Liu, C. Yan, J.A. Capobianco, Photon upconversion nanomaterials, Chem. Soc. Rev. 44 (2015) 1299–1301.
[90] D.K. Chatterjee, M.K. Gnanasammandhan, Y. Zhang, Small Upconverting Fluorescent Nanoparticles for Biomedical Applications, Small 6 (2010) 2781–2795.
[91] G. Chen, H. Qiu, P.N. Prasad, et al., Upconversion nanoparticles: design, nanochemistry, and applications in Theranostics, Chem. Rev. 114 (2014) 5161–5214.
[92] F. Wang, D. Banerjee, Y. Liu, et al., Upconversion nanoparticles in biological labeling, imaging, and therapy, Analyst 135 (2010) 1839–1854.
[93] D. Yang, C. Li, J. Lin, Multimodal cancer imaging using lanthanide-based upconverison nanoparticles, Nanomedicine-uk 10 (2015) 92.
[94] S. Yano, S. Hirohara, M. Obata, et al., Current states and future views in photodynamic therapy, J. Photochem. Photobiol. C Photochem. Rev. 12 (2011) 46–67.
[95] R.R. Allison, C.H. Sibata, Oncologic photodynamic therapy photosensitizers: a clinical review, Photodiagn. Photodyn. Ther. 7 (2010) 61–75.
[96] M.S. Saptista, J. Cadet, P.K. Mascio, et al., Type I and type II photosensitized oxidation reactions: guidelines and mechanistic pathways, Photochem. Photobiol. 93 (2017) 912–919.
[97] C.A. Robertson, D.H. Evans, H. Abrahamse, Photodynamic therapy (PDT): a short review on cellular mechanisms and cancer research applications for PDT, J. Photochem. Photobiol. B, Biol. 96 (2009) 1–8.
[98] L. Xia, X. Kong, X. Liu, et al., An upconversion nanoparticle-Zinc phthalocyanine based nanophotosensitizer for photodynamic therapy, Biomaterials 35 (2014) 4146–4156.
[99] X. Wang, K. Liu, G. Yang, et al., Near-infrared light triggered photodynamic therapy in combination with gene therapy using upconversion nanoparticles for effective cancer cell killing, Nanoscale 6 (2014) 9198–9205.
[100] L. Zeng, L. Xiang, W. Ren, et al., Multifunctional photosensitizer-conjugated core–shell, $Fe3O_4$@$NaYF_4$:Yb/Er nanocomplexes and their applications in T_2-weighted magnetic resonance/upconversion luminescence imaging and photodynamic therapy of cancer cells, RSC Adv. 3 (2013) 13915–13925.
[101] L. Zhang, L. Zeng, Y. Pan, et al., Inorganic photosensitizer coupled Gd-based upconversion luminescent nanocomposites for in vivo magnetic resonance imaging and near-infrared-responsive photodynamic therapy in cancers, Biomaterials 44 (2015) 82–90.
[102] L. Zeng, Y. Pan, R. Zou, et al., 808 nm-excited upconversion nanoprobes with low heating effect for targeted magnetic resonance imaging and high-efficacy photodynamic therapy in HER2-overexpressed breast cancer, Biomaterials 103 (2016) 116–127.
[103] L. Yuemei, W. Rui, X. Yanling, Wei Zheng, et al., Influence of silica surface coating on operated photodynamic therapy property of Yb^{3+}-Tm^{3+}:Ga(III)-Doped ZnO upconversion nanoparticles, Inorg. Chem. (2018), https://doi.org/10.1021/acs.inorgchem.8b01169.
[104] A. Punjabi, X. Wu, A. Tokatli-Apollon, et al., Amplifying the red-emission of upconverting nanoparticles for biocompatible clinically used prodrug-induced photodynamic therapy, ACS Nano 8 (2014) 10621–10630.
[105] J. Liu, L. Huang, X. Tian, et al., Magnetic and fluorescent Gd_2O_3:Yb^{3+}/ln^{3+} nanoparticles for simultaneous upconversion luminescence/MR dual modal imaging and NIR-induced photodynamic therapy, Int. J. Nanomed. Nanosurg. 12 (2017) 1–14.
[106] H. Sha, J.J.J. Noah, A.N.H. Viet, et al., Leveraging spectral matching between photosensitizers and upconversion nanoparticles for 808 nm-activated photodynamic therapy, Chem. Mater. 30 (2018) 3991–4000.
[107] J. Xu, L. Xu, C. Wang, et al., Near-infrared-Triggered photodynamic therapy with multi-tasking upconversion nanoparticles in combination with checkpoint blockade for immunotherapy of colorectal Cancer, ACS Nano 11 (2017) 4463–4474.
[108] H. Wang, R. Han, L. Yang, et al., Design and synthesis of core − Shell − Shell upconversion nanoparticles for NIR-Induced drug release, photodynamic therapy, and cell imaging, ACS Appl. Mater. Interfaces 8 (2016) 4416–4423.
[109] L. Liang, A. Care, R. Zhang, et al., Facile assembly of functional upconversion nanoparticles for targeted Cancer imaging and photodynamic therapy, ACS Appl. Mater. Interfaces 8 (2016) 11945–11953.
[110] S.R. Rout, R.K. Das, S. Nayak, et al., Highly hydrophilic luminescent magnetic mesoporous carbon nanospheres for controlled release of anticancer drug and multimodal imaging, Langmuir 32 (2016) 1611–1620.
[111] F. Zhang, G.B. Braun, A. Pallaoro, et al., Mesoporous multifunctional upconversion luminescent and magnetic "nanorattle" materials for targeted chemotherapy, Nano Lett. 12 (2012) 61–67.
[112] L. Cheng, K. Yang, Y. Li, et al., Facile preparation of multifunctional upconversion nanoprobes for multimodal imaging and dual-targeted photothermal therapy, Angew. Chemie Int. Ed. English 50 (2011) 7385–7390.
[113] L. Cheng, K. Yang, Y. Li, et al., Multifunctional nanoparticles for upconversion luminescence/ MR multimodal imaging and magnetically targeted photothermal therapy, Biomaterials 33 (2012) 2215–22122.
[114] B. Dong, S. Xu, J. Sun, et al., Multifunctional $NaYF_4$:Yb^{3+}, Er^{3+}@Ag core/shell nanocomposites: integration of upconversion imaging and photothermal therapy, J. Mater. Chem. 21 (2011) 6193–6200.

[115] X. Zhu, W. Feng, J. Chang, et al., Temperature-feedback upconversion nanocomposite for accurate photothermal therapy at facile temperature, Nat. Commun. 7 (2016) 10437.
[116] Y.I. Park, H.M. Kim, J.H. Kim, et al., Theranostic probe based on lanthanide-doped nanoparticles for simultaneous in vivo dual-modal imaging and photodynamic therapy, Adv. Mater. 24 (2012) 5755–5761.
[117] X. Huang, B. Li, C. Peng, et al., NaYF4:Yb/Er@PPy core–shell nanoplates: an imaging-guided multimodal platform for photothermal therapy of cancers, Nanoscale 8 (2016) 1040–1048.
[118] G. Jalani, R. Naccache, D.H. Rosenzweig, et al., Photocleavable hydrogel - coated upconverting nanoparticles: a multifunctional theranostic platform for NIR imaging and on-demand macromolecular delivery, J. Am. Chem. Soc. 138 (2016) 1078–1083.
[119] M. Sun, L. Xu, W. Ma, et al., Hierarchical plasmonic nanorods and upconversion core-satellite nanoassemblies for multimodal imaging-guided combination phototherapy, Adv. Mater. 28 (2016) 898–904.
[120] X. Ai, C.J.H. Ho, J. Aw, et al., In vivo covalent cross-linking of photon-converted rare-earth nanostructures for tumour localization and theranostics, Nat. Commun. 7 (2016) 10432.
[121] R. Lv, P. Yang, F. He, et al., A yolk-like multifunctional platform for multimodal imaging and synergistic therapy triggered by a single near-infrared light, ACS Nano 9 (2015) 1630–1647.
[122] S. Gai, P. Yang, C. Li, et al., Synthesis of magnetic, up-conversion luminescent, and mesoporous core-shell-Structured nanocomposites as drug carriers, Adv. Funct. Mater. 20 (2010) 1166–1172.
[123] G. Tian, Z. Gu, L. Zhou, et al., Mn^{2+} dopant-controlled synthesis of $NaYF_4$:Yb/Er upconversion nanoparticles for in vivo imaging and drug delivery, Adv. Mater. 24 (2012) 1226–1231.
[124] N.M. Idris, M.K.G. Jayakumar, A. Bansal, et al., Upconversion nanoparticles as versatile light nanotransducers for photoactivation applications, Chem. Soc. Rev. 44 (2015) 1449–1478.
[125] F.S. Collins, H. Varmus, A new initiative on precision medicine, New England J. Med. Surg. Collat. Branches Sci. 372 (2015) 793–795.
[126] J.L. Jameson, D.L. Longo, Precision medicine-personalized, problematic, and promising, Obstet. Gynecol. Surv. 372 (2015) 2229–2234.
[127] D. Yang, P. Ma, Z. Hou, et al., Current advances in lanthanide ion (Ln^{3+})-based upconversion nanomaterials for drug delivery, Chem. Soc. Rev. 44 (2015) 1416–1448.
[128] Z. Xu, C. Li, P. Ma, et al., Facile synthesis of an up-conversion luminescent and mesoporous Gd_2O_3: Er^{3+}@nSiO_2@mSiO_2 nanocomposite as a drug carrier, Nanoscale 3 (2011) 661–667.
[129] J. Liu, J. Bu, W. Bu, et al., Real-time in vivo quantitative monitoring of drug release by dual-mode magnetic resonance and upconverted luminescence imaging, Angew. Chemie Int. Ed. English 53 (2014) 4551–4555.
[130] C. Wang, L. Cheng, Z. Liu, Drug delivery with upconversion nanoparticles for multi-functional targeted cancer cell imaging and therapy, Biomaterials 32 (2011) 1110–1120.
[131] Y. Dai, H. Xiao, J. Liu, et al., In vivo multimodality imaging and Cancer therapy by near-infrared light-triggered trans-platinum pro-drug-Conjugated upconverison nanoparticles, J. Am. Chem. Soc. 135 (2013) 18920–18929.
[132] P. Ma, H. Xiao, X. Li, et al., Rational design of multifunctional upconversion nanocrystals/ polymer nanocomposites for cisplatin (IV) delivery and biomedical imaging, Adv. Mater. 25 (2013) 4898–4905.
[133] S.Y. Choi, S.H. Baek, S.J. Chang, et al., Synthesis of upconversion nanoparticles conjugated with grapheme oxide quantum dots and their use against cancer cell imaging and photodynamic therapy, Biosens. Bioelectron. 93 (2017) 267–273.
[134] Y. Dan, X. Jiating, Y. Guixin, et al., Metal-organic frameworks join hands to create an anti-cancer nanoplatform based on 808 nm light driving up-conversion nanoparticles, Chem. Eng. J. 344 (2018) 363–374.
[135] C. Wang, L. Cheng, Z. Liu, Upconversion nanoparticles for photodynamic therapy and other Cancer therapeutics, Theranostics 3 (2013) 317–330.
[136] L. Shao, T. Boshi, W. Shuyi, et al., pH-sensitive polymer-gated multifunctional upconversion $NaYF_4$:Yb/Er@mSiO_2 nanocomposite for oral drug delivery, Microporous Mesoporous Mater. 264 (2018) 151–158.
[137] J.C. Boyer, Veggel FCJMv, Absolute quantum yield measurements of colloidal $NaYF_4$:Er^{3+},Yb^{3+} upconverting nanoparticles, Nanoscale 2 (2010) 1417–1419.
[138] P. Lei, R. An, X. Zhai, et al., Benefits of surfactant effects on quantum efficiency enhancement and temperature sensing behavior of $NaBiF_4$ upconversion nanoparticles, J. Mater. Chem. C Mater. Opt. Electron. Devices 5 (2017) 9659–9665.